CLASSIFICATION OF PLANTS USING IMAGES OF THEIR LEAVES

A Thesis
by
BIVA SHRESTHA
December 2010

APPROVED BY

_____
Rahman Tashakkori
Chairperson, Thesis Committee

_____
Alice A. McRae
Member, Thesis Committee

_____
Zack E. Murrell
Member, Thesis Committee

_____
James T. Wilkes
Chairperson, Computer Science

_____
Edelma Huntley
Dean, Research and Graduate Studies

CLASSIFICATION OF PLANTS USING IMAGES OF THEIR LEAVES

A Thesis
by
BIVA SHRESTHA
December 2010

Submitted to the Graduate School
Appalachian State University
in partial fulfillment of the requirements for the degree of
MASTER OF SCIENCE

December 2010
Major Department: Computer Science

ABSTRACT

CLASSIFICATION OF PLANTS USING IMAGES OF THEIR LEAVES

Biva Shrestha

M.S., Appalachian State University

Thesis Chairperson: Rahman Tashakkori

Plant recognition is a matter of interest for scientists as well as laymen. Computer aided technologies can make the process of plant recognition much easier; botanists use morphological features of plants to recognize them. These features can also be used as a basis for an automated classification tool. For example, images of leaves of different plants can be studied to determine effective algorithms that could be used in classifying different plants. In this thesis, those salient features of plant leaves are studied that may be used as a basis for plant classification and recognition. These features are independent of leaf maturity and image translation, rotation and scaling and are studied to develop an approach that produces the best classification algorithm. First, the developed algorithms are used to classify a training set of images; then, a testing set of images is used for verifying the classification algorithms.

ACKNOWLEDGMENTS

First and foremost, I would like to express my deepest gratitude to my advisor, Dr. Rahman Tashakkori, for his continuous support and guidance throughout my M.S. pursuit. His love towards research work and innovation was the biggest motivational factor for me. He taught me to view a problem as an adventure which has led me to enjoy my research while meeting the challenges. Without his guidance and persistent help this thesis would not have been possible.

I would also like to express my heartfelt thanks to my co-advisors, Dr. Alice McRae and Dr. Zack Murrell, for their valuable advice.

I would like to thank my family for continually believing in me. They have always encouraged me never to give up in pursuing my goals. Without their love and presence the successes as well as the failures would have been meaningless.

Finally, I would like to thank my best friend, my guide and my husband, Unnati Ojha, for always being there for me to discuss and aid me through difficult situations. Without his help, care and understanding, all of my achievements would have been unreached.

TABLE OF CONTENTS

LIST OF TABLES

LIST OF FIGURES

CHAPTER 1: INTRODUCTION

1.1. Computer Vision

This thesis focuses on automation through computer vision. Computer vision is concerned with the theory behind artificial systems that extract information from images. The image data can take many forms, such as video sequences, views from multiple cameras, or multi-dimensional data from a medical scanner. In other words, computer vision is the science and technology of machines that have the ability to see. Snyder [1] describes the term computer vision as "The process whereby a machine, usually a digital computer, automatically processes an image and reports 'what is in the image', i.e., it recognizes the content of the image. Often the content may be a machine part, and the objective is not only to locate the part, but to inspect it as well." Computer vision, also known as machine vision, consists of three parts: measurement of features, pattern classification based on those features, and pattern recognition. This thesis was conducted to develop a system that extracts different features from a leaf image and classifies different classes of leaves based on the extracted features. Furthermore, the system uses the results of the classification scheme in identifying the class of new leaf images.

1.2. Measurement/Extraction of Features

Image processing technologies are used to extract a set of features/measurements that characterize or represent the image. The values of these features provide a concise

representation about the information in the image. For example, a set of features that characterize a triangle could be the length of each side of the triangle.

1.3. Pattern Classification

Pattern classification is the organization of patterns into groups of patterns sharing the same set of properties. Given a set of measurements of an unknown object and the knowledge of possible classes to which an object may belong, a decision about to which class the unknown object belongs could be made. For example, if information about the length of sides of an unknown triangle is extracted, a decision on whether the unknown triangle is an equilateral, isosceles or scalene triangle can be made. Similarly, if a set of features/measurements is extracted from a leaf, a decision about the possible class of the leaf can be made. Pattern classification may be statistical or syntactic.

Statistical classification is the classification of individual items into groups based on quantitative information of one or more features/measurements of the item and based on a training set of previously classified items. An example of this type of classification is clustering; this study uses clustering for pattern classification.

Syntactic classification (Structural classification) is the classification of individual items based on a structure in the pattern of the measurements. Items are classified syntactically only if there is a clear structure in the pattern of the measurements.

1.4. Pattern Recognition

Pattern recognition is the process of classifying data or patterns based on the knowledge/information extracted from patterns. The patterns to be classified are usually

groups of measurements or observations defining points in an appropriate multidimensional space. In this thesis, pattern recognition is implemented on a set of test images in order to validate and evaluate the performance of the underlying classification scheme.

1.5. Applications of Computer Vision

Some applications of computer vision are face recognition, fingerprint recognition, image-based searching, optical character recognition, remote sensing, and number plate recognition.

This thesis is highly inspired by the real world applications of computer vision. The key idea of most of these technologies is automation. Automation is an interdisciplinary concept that uses technologies in the computer world to simplify complex issues in other disciplines or in everyday life. This research focuses on using image processing to automate classification and perform plant recognition based on the images of the leaves. Automatic plant classification and recognition can assist botanists in their study as well as help laymen in identifying and studying plants. Different shape-related features were extracted from these images using image processing algorithms. Depending on these features, a statistical classification of plants was conducted. The classification scheme was then validated using a set of test images.

1.6. Thesis Organization

This thesis is organized into six chapters: Introduction, Related Work, Image Processing, Methodology, Results, Conclusions and Future Recommendations. The Related Work chapter gives a short preview on similar studies that have been done

previously and which may be grouped into different categories. The categories are: extraction of single feature of leaf or flower, leaf image matching of single plant species, image-based plant recognition, and image-based plant classification. The Methodology chapter describes different image processing and feature extraction techniques used and the classification algorithm implemented for correctly identifying the plants based on their leaves. The Results chapter presents the results of the research and discusses the significance of extracted features in classifying plants. Finally, the Conclusions and Future Recommendations chapter summarizes the outcomes of this study, and discusses possible modifications and improvements.

CHAPTER 2: RELATED WORK

Modern plant taxonomy starts with the Linnaeus' system of classification [2]. This is a plant classification and nomenclature system and is currently used, albeit in a revised version. In this classification system plants are classified based on their similarity and dissimilarity. Linnaeus' classification and nomenclature gives scientific names to plants and is a universal language for botanists. Classification and nomenclature of plants is useful only if plants can be recognized. Botanists recognize plants based on their knowledge and expertise, but for laymen plant recognition is still a complicated task. Plant recognition can be made simpler by using computer aided automation. A plant recognition system should be based on a plant classification system because there are more than one-half million of plants inhabiting the Earth and recognition without classification is a complex task. Hence, this thesis focuses on an automated plant classification system.

Studies have been conducted in the past decade on automation of plant classification and recognition. A handful of these studies were about the extraction of a single feature from the image of a plant part such as the leaf, or the flower. Some studies were about the extraction of multiple features but from a single family of plants. Some studies focused on image-based plant classification, while others focused on image-based plant recognition. Warren [3] introduced an automatic computerized system that used as

its input 10 images of each Chrysanthemum species for testing the variation in the images. In this study, features such as shape, size and color of the flower, petal, and leaf were described mathematically. Different rose features were extracted and used in the recognition scheme for pattern recognition. The study, however, was limited to Chrysanthemum species only. Miao *et al*., [4] proposed an evidence-theory-based rose plant classification using different features of roses. In another study by Heymans *et al*., [5], a back-propagating neural network approach was used to distinguish different leaves of Opuntia species. Again, the study was limited only to the variety of the Opuntia family. Saitoh and Kaneko [6] studied an automatic method for recognizing wild flowers. This recognition required two images: a frontal flower image and a leaf image taken by a digital camera. Seventeen features, eight from the flower and nine from the leaf, were fed to a neural network. This research yielded an accuracy of 95% on 20 pairs of pictures from 16 wild flowers. These studies dealt with a single or group of similar plant species only.

Some studies focused on extraction of vein features. Li *et al*., [7] used snake techniques [8] with cellular neural networks (CNN) to extract the leaf venation feature from leaf images. Fu and Chi [9] also studied the extraction of leaf venation feature using neural network. Their methodology involved a preliminary segmentation which is based on the intensity histogram that coarsely determined the vein regions. This was followed by segmentation using a trained artificial neural network (ANN) classifier with 10 features extracted from a window centered on pixels within the object. Qi and Yang [10] studied the extraction of saw tooth feature of the edges of a leaf based on support vector machine. These studies were limited to the extraction of a single feature only.

Some other studies focused on image-based plant recognition via shape matching. Nam *et al*., [11] studied a shape-based leaf image retrieval system using two novel approaches, namely, an improved maximum power point (MPP) algorithm and a revised dynamic matching method. In his approach, Nam, et al, used a region-based shape representation technique to define the shapes of the leaf. Certain points of interest were evaluated and the distances between the points were taken as the features for image matching. Fu and Chi, [12] studied a two-stage approach for leaf image retrieval using simple shape features such as centroid-contour distance (CCD) curve, eccentricity, and angle code histogram (ACH). Their first stage reduced the query space by eliminating images dissimilar to the query image based on eccentricity. The second stage retrieved the best match based on all three features. Their approach showed a better result than that of an exhaustive search. The study was focused on image retrieval and did not contain the details about the classification methodology used. Gu *et al*., [13] used a combination of wavelet transform and Gaussian interpolation to extract the leaf venation and contour of leaf from its image and derived run length features based on the image. The plants were then classified based on the extracted and derived features using 1-NN, k-NN and radial basis probabilistic neural network (RBPNN). Du *et al*., [14] used move median centers (MMC) hypersphere classifier to classify plants based on shape-related features of leaf such as aspect ratio, rectangularity, area ratio of convex hull, perimeter ratio of convex hull, sphericity, circularity, eccentricity, form factor, and invariant moments.

Some works in the past studied algorithms for image-based plant classification. The images used in these studies were mostly leaf images and the features extracted were shape features. Fu *et al*., [15] proposed an ontology based leaf classification using

information from leaf images. Their ontology had two main branches, namely, shape and venation. Shape was classified according to lobation and margin. Lobation and margin had further sub branches describing the structure of lobe or margin. Their study, however, did not reveal the number of test cases used and its overall success rate. Wang *et al*., [16] used a MMC hypersphere classifier for classifying plants based on certain leaf features. First, image segmentation was applied to the leaf images; then eight geometric features such as rectangularity, circularity, eccentricity, and seven moment invariants were extracted for classification. Finally, a hypersphere classifier was used to address these shape features. Wu *et al*., [17] used a probabilistic neural network for classification of leaf images based on 12 leaf features. A principal component analysis (PCA) was used for reducing the 12 dimensions into five dimensions for faster processing. The 12 features used were physiological length, physiological width, leaf area, leaf perimeter, smooth factor, aspect ratio, form factor, rectangularity, narrow factor, perimeter ratio of diameter, perimeter ratio of physiological length and physiological width, and vein features. The use of scale variant features such as physiological length, physiological width, area, and perimeter might constrain this approach into using standard size for the leaf image. If a standard size image is not used then the features of the same leaf vary with different sizes images. Since it is the same leaf, the value of all the features are expected to be same. The values for these features vary for different scaled versions of the same leaf image. In this research features used are scaling, translation and rotation invariant. In addition, a distinct shape feature, skeleton, is introduced for classification of leaves.

CHAPTER 3: IMAGE PROCESSING

3.1. Introduction

An image can be defined as a two-dimensional function, $f(x, y)$, where x and y are spatial coordinates, and f is the amplitude at any pair of coordinates (x, y) [1]. A digital image is a two-dimensional matrix with discrete value for position as well as intensity. Pixels represent the position and the value of the pixel represents the intensity at that position. A binary image is an image with only two intensity values, zero or one. A grayscale image is an image whose intensities are a range of values representing different levels of gray. There are various formats of a colored image. In red-green-blue (RGB) format, the intensity at each pixel is represented by a vector that contains the blue, red and green levels.

Digital image processing refers to the processing of digital images by means of a computer. There is a vast range of applications of digital image processing; two examples are X-ray imaging and Gamma-ray imaging. Digital image processing is also used as a basis for image-based automatic systems such as automatic face recognition, fingerprint recognition, etc. This thesis focuses on using digital image processing for the purpose of automation. Digital images of plant leaves are processed using various algorithms to extract shape related features. Finally, the classification is done based on the extracted

features. Some terminologies that address various features are explained in Sec. 3.2 through Sec. 3.6.

3.2. Convex Hull and Convex Hull Ratio

Convex hull, *H*, of an arbitrary set of points, *S*, is the smallest convex set containing *S*. Hence, all the points in *S* are either inside *H* or on *H*. The red line on Fig. 3.1 illustrates an example of a convex hull for the set of blue points.

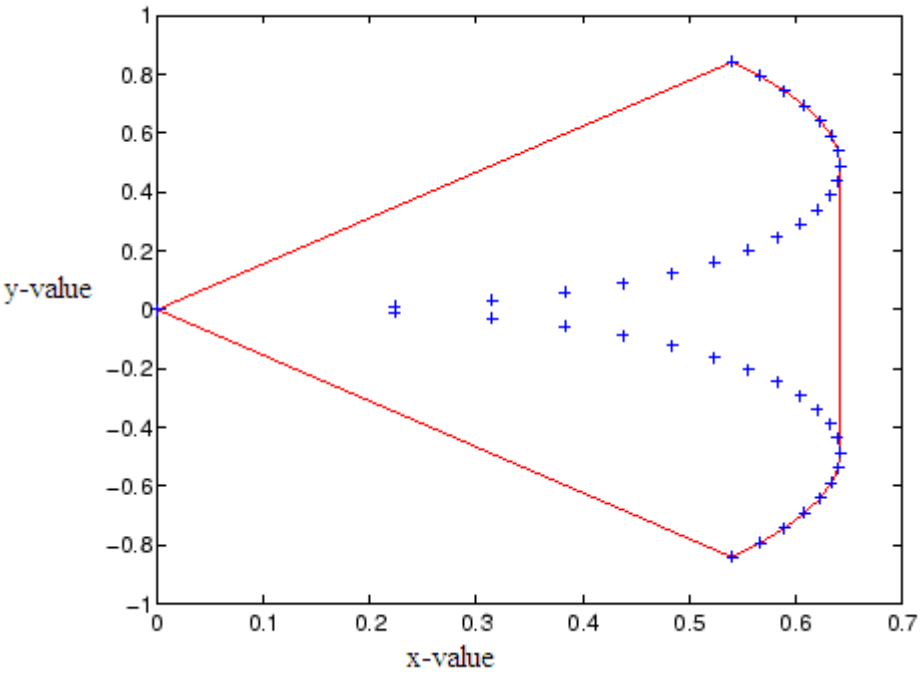

Fig. 3.1: Illustration of a convex hull

The convex hull ratio is the ratio of the area of the foreground of an image to the area of the convex hull. The area of the foreground is the number of pixels contained in the foreground of the image. Similarly, the area of the convex hull is the area contained within the convex hull. The algorithm for extracting the convex hull is presented in Sec. 4.3.1.

3.3. Eccentricity

Eccentricity for an ellipse with major axis *Ma* and minor axis *Mi* is defined by the ratio (3.1).

$$Eccentricity = \sqrt{\frac{Ma^2 - Mi^2}{Ma}} \tag{3.1}$$

In order to extract the eccentricity of an object in a digital image, the best fitting ellipse is first evaluated. The best fitting ellipse is the ellipse for which the sum of the squares of the distances to the given points is minimal. In other words, the best fitting ellipse is an ellipse that best fits to the data points contained in the region of interest. Fig. 3.2 illustrates a best fitting ellipse to a polygon. It also illustrates the major axis, *Ma* and the minor axis, *Mi* of the best fitting ellipse. The algorithm for the extraction of eccentricity is presented in Sec. 4.3.3.

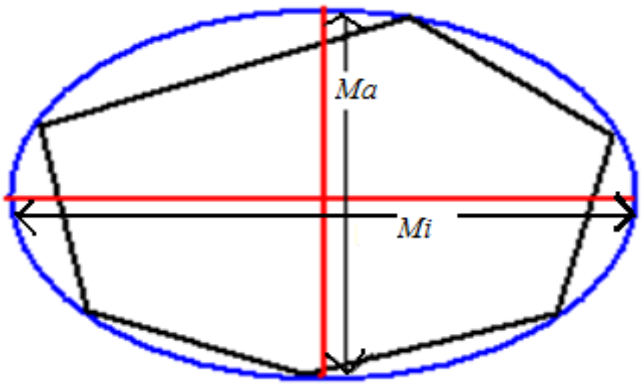

Fig. 3.2: The best fitting ellipse to a polygon with its major and minor axes

3.4. Isoperimetric Quotient

Denoting P as the perimeter of the foreground of an image and A as the area of the foreground, the isoperimetric quotient is given by (3.2). The algorithm for extraction of isoperimetric quotient is discussed in Sec. 4.3.2.

$$Isoperemetric\ quoitent = \frac{4\pi A}{P^2} \tag{3.2}$$

3.5. Skeleton

According to Talea [18] the skeleton of a shape is a compact representation of 2D or 3D such that it preserves many of the topological and size characteristics. Mathematically, the skeleton is the locus of centers of the maximum disk contained in the original object [19]-[20]. As illustrated in Fig. 3.3, the line joining the centers of all the disks touching at least two boundary points of the shape gives the skeleton of the shape. Talea proposes three methods for the calculation of skeleton:

- Morphological Method
- Geometric Method
- Distance Transform

The morphological method, also known as morphological thinning, iteratively peels off the boundary layer, identifying points whose removal does not affect the object's topology. This method has the disadvantage of missing connectivity.

The geometric method proposed by Ogniewicz [21] is a medial axis transform (MAT) algorithm. For each point p in an arbitrary region R, its closest neighbor in the boundary of R, is found and if p has more than one such neighbor, then p is said to belong

to the MAT skeleton of *R.* The MAT algorithm is computationally exhaustive because for each foreground pixel, distances from all the boundary pixels must be calculated.

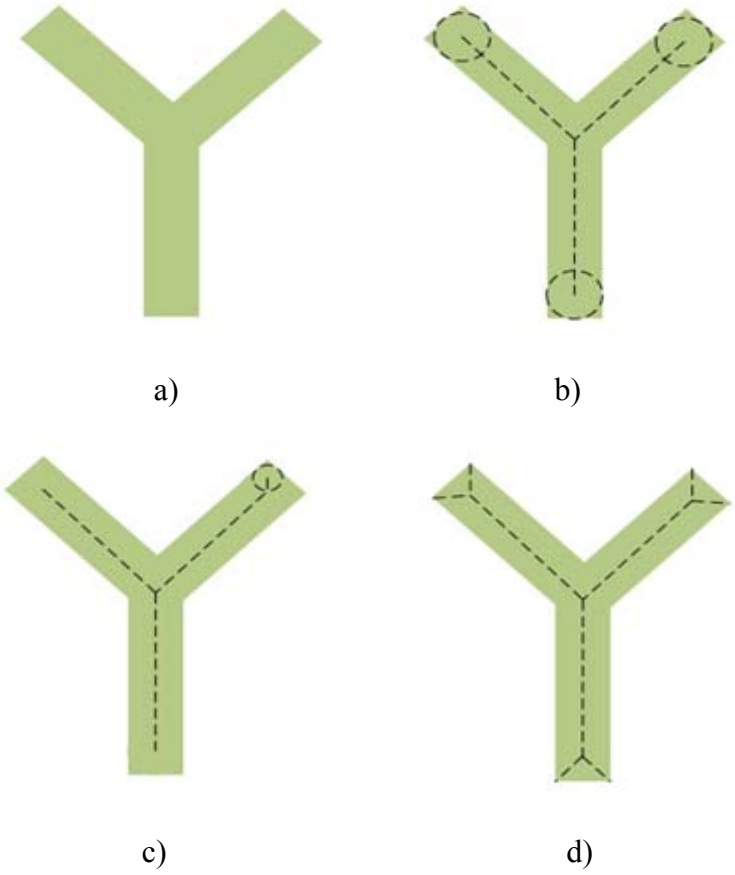

Fig. 3.3: a) An arbitrary object, b) and c) various positions of maximum disks with centers on skeleton of the object, d) the complete skeleton

A better approach to skeleton development is the distance transform (DT) method. In this method, each foreground pixel is assigned a value depending on its distance from the boundary pixel. The pixels having a local minimal value are detected as skeletal points. A robust and efficient implementation of distance transform is introduced by Sethian [22]. According to Sethian, the skeleton lies along the singularities in the DT or in other words the skeletal points coincide with the points where the moving boundary

collapses onto itself. This thesis uses an augmented fast-marching method proposed by Talea [18] for the calculation of the skeleton. The algorithm is described in Chap. 4.

3.6. Clustering

Clustering or cluster analysis is a classification method by which a set of data points or observations are classified into subsets or clusters such that similar data points lie in the same cluster. It is a common technique for statistical data analysis and is used in machine vision and image analysis. One of the clustering techniques, K-means clustering, is used in this thesis for the purpose of leaf image classification. K-means clustering is an algorithm to classify the objects based on attributes/features into K number of groups where K is a positive integer. The grouping is done by minimizing the sum of squares of distances between data and the corresponding cluster centroid. K-means clustering is a supervised learning algorithm and requires a prior knowledge of the number of clusters.

CHAPTER 4: METHODOLOGY

4.1. System Overview

The primary source of leaf images is the Irvin Watson Carpenter, Jr. Herbarium located in the Department of Biology at Appalachian State University. Images are also taken from the Robert K. Godfrey Herbarium at Florida State University, and the University of North Carolina Herbarium. These herbaria have databases of specimens, containing the images of plant parts, mostly with leaves and flowers. Fig. 4.1 illustrates a specimen from I. W. Carpenter, Jr. Herbarium. These images are cropped manually to get images of individual leaves that are used in this thesis. As illustrated in Fig. 4.2 the following four steps are used for implementing the automatic plant recognition system:

- Image Preprocessing
- Measurement/Extraction of Features
- Pattern Classification
- Pattern Recognition

Fig. 4.1: A sample plant specimen from I. W. Carpenter, Jr. Herbarium

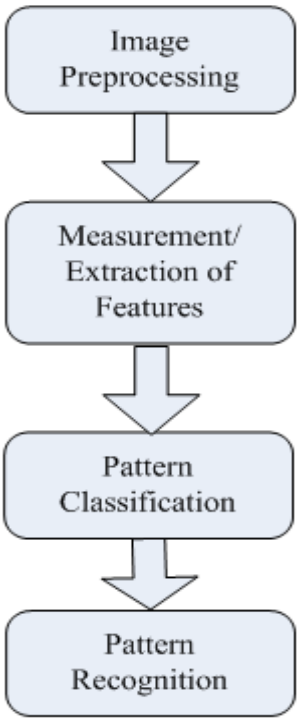

Fig. 4.2: Steps involved in image preprocessing

4.2. Image Preprocessing

The images acquired from the Irvin Watson Carpenter, Jr. Herbarium are not suitable for image processing because they are a large size (up to 17 Megabytes) and they are RGB images. It is computationally expensive to process a 17 Megabytes, colored image. Extraction of features is simpler with binary images because all the pixel values in a binary image can either be zero or one, hence, computations become simpler. Thus, the images are preprocessed and converted into smaller size files in binary format without the loss of any morphological (shape related) information. The steps involved in image preprocessing are shown in Fig. 4.3.

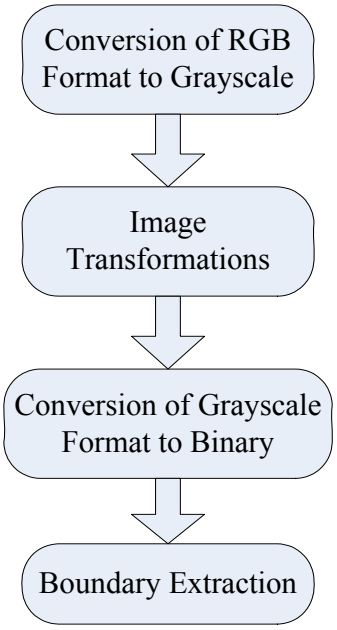

Fig. 4.3: Four steps of methodology

4.2.1. Conversion of RGB Format to Grayscale

For each pixel in a digital RGB image, the respective grayscale value can be found by two methods: averaging and weighted averaging. Assuming *R*, *G* and *B*

represent the respective intensities for red, green and blue channel of a pixel, then the averaging algorithm would calculate the respective grayscale intensity, *GI* using (4.1).

$$GI = \frac{R + G + B}{3} \tag{4.1}$$

The weighted averaging method is similar to the averaging method except that some weighting factor is given to each of the color intensities. The weights used in this research are defined in (4.2).

$$GI = 0.2989 * R + 0.5870 * G + 0.1140 * B \tag{4.2}$$

Fig. 4.4 illustrates an arbitrary RGB image and the grayscale images obtained after using weighted averaging and averaging techniques. The weighted averaging method produced an image that better distinguishes between the foreground and background pixels and the weights used can only produce an optimal result.

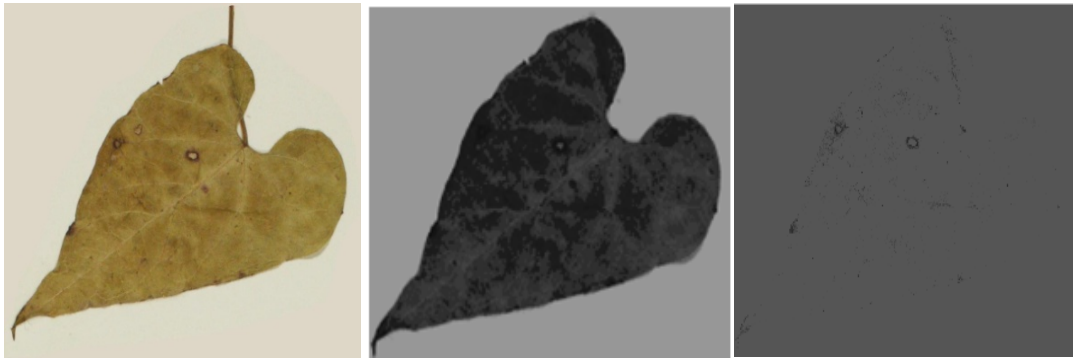

a) b) c)

Fig. 4.4: a) An arbitrary RGB image, b) Grayscale equivalent using weighted averaging, c) Grayscale equivalent using averaging

4.2.2. Image Transformations

The transformation of coordinates or pixels in an image by performing operations such as scaling, rotation, translation, and shear can be expressed in a general form as shown in (4.3)

$$\begin{bmatrix} x \\ y \\ 1 \end{bmatrix} = T \begin{bmatrix} v \\ w \\ 1 \end{bmatrix} \tag{4.3}$$

where, (v, w) is pixel in the original image, (x, y) is the corresponding pixel coordinate in the transformed image and T is the transformation matrix. In this thesis scaling transformation is used to reduce the size of the image file. An example of scaling is reducing the image size by half, which is shown in (4.4)

$$\begin{bmatrix} x \\ y \\ 1 \end{bmatrix} = \begin{bmatrix} \frac{1}{2} & 0 & 0 \\ 0 & \frac{1}{2} & 0 \\ 0 & 0 & 1 \end{bmatrix} \begin{bmatrix} v \\ w \\ 1 \end{bmatrix} \tag{4.4}$$

In this research, the inverse mapping algorithm is used for image resizing. The output pixel at each location, (x, y), is computed as an accumulated contribution of relevant input pixels which are the neighboring pixels. The output pixel value is determined by interpolating between the nearest input pixels.

4.2.3. Conversion of Grayscale Format to Binary

Once a grayscale image of reduced size is obtained, it is converted to binary format. To convert a grayscale image into a binary image, Otsu's [23] method of automatic thresholding is used. During the thresholding process, pixels in an image are

marked as foreground if their values are larger than some threshold and as background otherwise. The shape of the histogram is used for automatic thresholding and the threshold is chosen so as to minimize the interclass variance of the black and white pixels.

4.2.4. Boundary Extraction

The Canny edge detector is used for edge detection and extraction of the region of interest. The Canny edge detection algorithm consists of four basic steps:

- smoothing the input image with a Gaussian filter
- computing the gradient magnitude and angle images.
- using double thresholding and connectivity analysis to detect and link edges.
- applying non-maxima suppression to the gradient magnitude image.

Step 1: Smoothing the input image with Gaussian filter

A 2-D Gaussian function, G, expressed by (4.5) is used for image smoothing.

$$G(x,y) = \frac{1}{2\pi\sigma^2} e^{-\frac{x^2+y^2}{2a^2}} \tag{4.5}$$

where, $a > 0$, is a constant, σ is Euler's constant, and $f(x,y)$ denotes the input image. If $G(a, b)$ denotes a discrete Gaussian filter of size m by n, the smoothened image, $f_s(i, j)$ is formed by convolving G and f and the intensity value at pixel (i, j) is given by (4.6).

$$f_s(i,j) = \sum_{a=1}^{m}\sum_{b=1}^{n} f(i-a, j-b)G(a,b) \tag{4.6}$$

A Gaussian filter has an impulse response of Gaussian nature.

Fig. 4.5 shows the discrete Gaussian filter used in this research.

$\frac{1}{273}\times$	1	4	7	4	1
	4	16	26	16	4
	7	26	41	26	7
	4	16	26	16	4
	1	4	7	4	1

Fig. 4.5: A Gaussian filter

Step 2: Computing the gradient magnitude and angle of images

Smoothing is followed by computing the gradient magnitude and angle at each pixel (x, y) in the image. The gradient and angle are computed using (4.7).

$$G(x,y) = e^{-\frac{x^2+y^2}{2a^2}}$$
$$\alpha(x,y) = \tan^{-1}\left[\frac{g_x}{g_y}\right] \tag{4.7}$$

where, $G(x,y)$ is the magnitude at pixel (x,y) and $\alpha(x,y)$ is the gradient angle at pixel (x,y).

Step 3: Using double thresholding to detect and link edges

The final step involves reducing the number of the false edge points. The Canny edge detector [24] uses two thresholds for reducing the false edges, contrary to some other algorithms that use only one. Use of a single threshold can result in inaccuracy because a high threshold detects some false edges and a low threshold eliminates some valid edges and therefore, hysteresis thresholding with a low threshold *TL* and a high threshold *TH* is used. Pixels with a gradient magnitude $D < TL$ and $D > TH$ are discarded

immediately; however, pixels with a magnitude D, such that $TL \leq D < TH$, are kept intact.

Step 4: Applying non-maxima suppression to the gradient image

Since the edges are detected using a gradient, they are not one pixel thick. They are made one pixel thick by finding the local maxima around the edges. Non-maxima suppression is used for thinning the edges. Non-maxima suppression only keeps those pixels in the edge with the highest gradient magnitude. As illustrated in Fig. 4.6, each pixel (x, y) is examined for the following orientations:

- if the direction of (x, y) is between -22.5° to 22.5° or from -157.5° to 157.5°, then it lies in the vertical border;
- if the direction of (x, y) is between 67.5° to 112.5° or -67.5° to -112.5°, then it lies in the horizontal border.

For a pixel in the vertical border, all of its vertical neighbors are examined. If the pixel is in the horizontal border, pixels in its horizontal neighborhood are examined. If (x, y) has a magnitude greater than the magnitude of all the neighbors examined, then it is kept intact, otherwise it is removed from the edge.

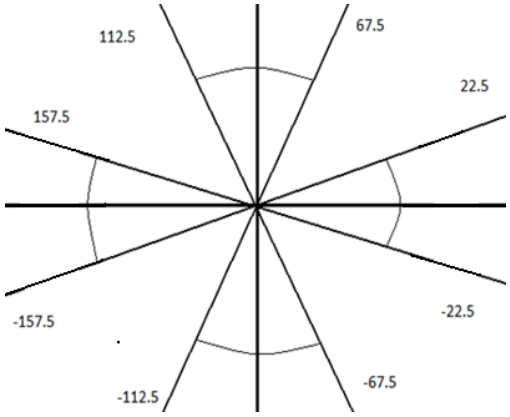

Fig. 4.6: Separation of angles for determining a vertical/horizontal neighbor in non-maxima suppression

4.3. Measurement/Extraction of Features

It is obvious that the most distinguishing feature of a plant's leaf is its shape. The shape of a leaf is invariant to plant maturity unlike the length, width, area, shape and other features, which might vary with maturity, climate or location. A set of features that best describe the shape of a leaf is the matter of interest in this research. The following features are used for classification of leaves: convex hull ratio, isoperimetric quotient, eccentricity, aspect ratio, and skeleton. The process of feature extraction is shown in Fig. 4.7.

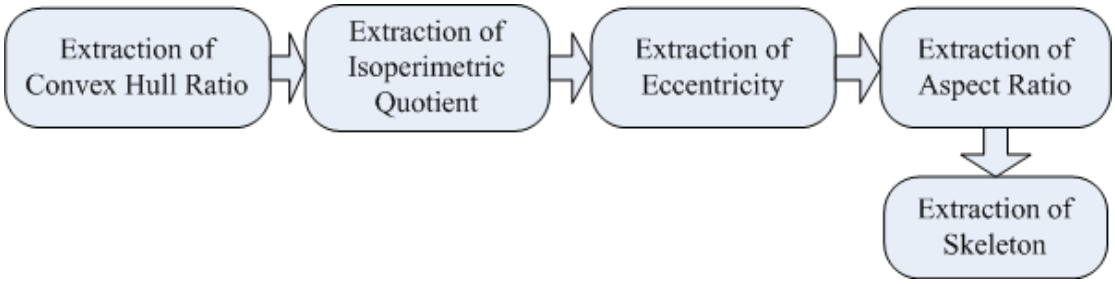

Fig. 4.7: Feature extraction process

4.3.1. Extraction of Convex Hull Ratio

Convex hull ratio requires two spatial parameters to be calculated: i) the area of the leaf, and ii) the area of the convex hull on the leaf. The area of the leaf is calculated as the number of pixels in the foreground of the binary image of the leaf. The area of the convex hull is calculated by counting the number of pixels enclosed by the hull.

To draw the convex hull, Andrew's monotone chain algorithm [25] is used, which is a variation of Graham's scan algorithm [26]. Like the Graham's scan, Andrew's monotone chain algorithm consists of sorting and computation. In both algorithms the first phase, sorting phase, has same complexity. However, the computational phase of monotone chain algorithm is equivalent to the worst case scenario of Graham's computational phase. Unlike Andrew's monotone chain algorithm, Graham's scan examines all the points for the calculation of the convex hull and hence has higher computational requirements.

Fig. 4.8 shows the process involved in Andrew's monotone chain algorithm. In this algorithm, a set of points $S = \{P_0, P_1, P_2 \ldots P_n\}$ are ordered according to increasing x-coordinate with coordinates having the same x value sorted in the increasing order of y value. As illustrated in Fig. 4.8, x_{min} and x_{max} are assumed to be the minimum and the maximum value for x. P_{--} is assumed to be the point with smallest y value among the points (x, y), with $x = x_{min}$. Similarly, the point with the largest y value among the points with $x = x_{min}$ is assumed to be P_{+-} . Also, P_{+-} and P_{++} are the points with $x = x_{max}$ but with the smallest and the largest y value, respectively. In Fig. 4.8, P_{++} and P_{+-} denote the same point because there is only one point with $x = x_{max}$. Two points denoted by P_{--} and P_{+-} are

joined to define a lower line L_{min}. Similarly, P_{-+} and P_{++} are joined to define an upper line L_{max}.

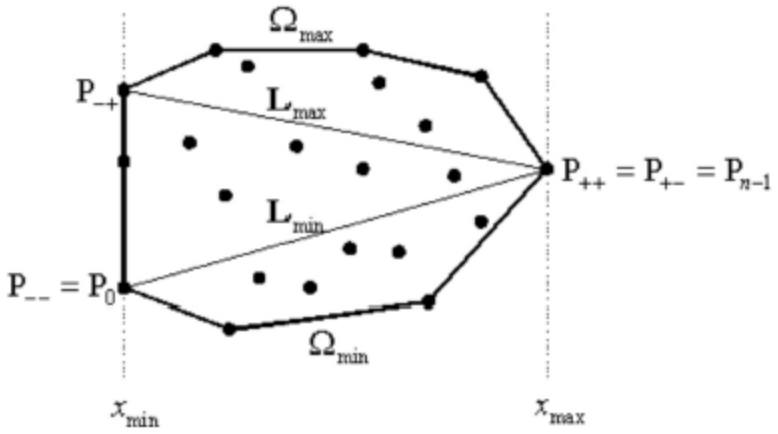

Fig. 4.8: Convex hull by Andrew's monotone chain algorithm

The computational part of the implementation consists of constructing a lower convex vertex chain Ω_{min} below L_{min} and an upper convex vertex chain Ω_{max} above L_{max}. The construction of the lower chain, Ω_{min} starts with pushing point P_{--} on a stack. The points of S below the lower line L_{min} are processed in sequence. The next point P_k below L_{min} is pushed onto the stack if the stack has only one point, i.e., P_{--}. Otherwise, the algorithm determines whether P_k is on the left of the line between the top two points on the stack, in which case, P_k is pushed onto the stack. Alternatively, the top of the stack is popped, and P_k is pushed onto the stack. After all points are processed, P_{+-} is pushed onto the stack to complete the lower convex chain. The lower convex chain is formed by joining the points in the stack.

The upper convex chain Ω_{max} is constructed in a similar manner, but S is scanned in reverse order $\{P_{n-1}, P_{n-2}, ..., P_0\}$.The algorithm starts with pushing P_{++}, and only the

points above L_{max} are scanned. Once the two hull chains are determined, they are joined to form the complete convex hull.

4.3.2. Extraction of Isoperimetric Quotient

Extraction of the isoperimetric quotient required extraction of the area and the perimeter of leaves. Given a binary leaf image, the area is calculated as the number of pixels in the foreground. Canny edge detector is used to get the edge image for the foreground region and perimeter is calculated as the number of pixels in the boundary of the foreground region.

4.3.3. Extraction of Eccentricity

For the extraction of eccentricity, the best fitting ellipse is first estimated using a region-based method. Unlike a boundary-based method, which uses boundary information to find the best fit, this region-based method uses the moments of a shape to estimate the best fitting ellipse. Region-based methods are faster because they are not affected by the irregularities of the shape.

For a region $f(x, y)$ that represents a leaf, the central moment is calculated using (4.8).

$$U_{pq} = \iint_g f(x-\bar{x})^p (y-\bar{y})^q \, dxdy \tag{4.8}$$

where,

$$\bar{x} = \frac{m_{10}}{m_{00}} \tag{4.9}$$

$$\bar{y} = \frac{m_{01}}{m_{00}} \tag{4.10}$$

and $(\bar{x}, \bar{y})$ represents the centroid of the region *f*. (m_{10},m_{01}) is the sum of *x*-coordinates and *y*-coordinates of points in the foreground and m_{00} is the area of *f*. The first six central moments are expressed as shown in (4.11) through (4.15).

$$u_{00} = m_{00} \tag{4.11}$$

$$u_{10} = u_{01} = 0 \tag{4.12}$$

$$u_{20} = m_{20} - \frac{m^2_{10}}{m_{00}} \tag{4.13}$$

$$u_{02} = m_{02} - \frac{m^2_{01}}{m_{00}} \tag{4.14}$$

$$u_{11} = m_{11} - \frac{m_{10} m_{01}}{m_{00}} \tag{4.15}$$

The normalized central moments are defined using (4.16).

$$n_{pq} = \frac{u_{pq}}{u^{\gamma}_{00}} \tag{4.16}$$

where,

$$\gamma = \frac{p+q}{2} + 1 \tag{4.17}$$

The central moments are used to define the best fit ellipse. For an arbitrary shape oriented at an angle *Ø*, with minor axis, *a*, and major axis, *b*, the values for these three parameters are calculated using (4.18), (4.19) and (4.20), respectively.

$$a = \sqrt{\frac{2(u_0 + u_{02} + \Delta)}{u_{11}}} \tag{4.18}$$

$$b = \sqrt{\frac{2(u_{20} + u_{02} - \Delta)}{u_{11}}} \tag{4.19}$$

$$\phi = \frac{1}{2}\tan^{-1}\left(\frac{2u_{11}}{u_{20}-u_{02}}\right) \tag{4.20}$$

where,

$$\Delta = \sqrt{4u^2_{11} + \left(u_{20}-u_{02}\right)^2} \tag{4.21}$$

4.3.4. Extraction of Aspect Ratio

For a rectangular shape, aspect ratio is the ratio of its breadth by length. Since leaves have irregular shapes, their aspect ratio is defined as the ratio of the minor axis to the major axis of the best fitting ellipse.

4.3.5. Extraction of Skeleton

The skeleton of a leaf is extracted using the augmented fast marching method (AFMM) [18]. AFMM is based on the observation that skeletal points are always generated by compact boundary points that collapse as the moving fronts advance inward starting across the boundary. As the name suggests, augmented fast marching is a development in the fast marching method [22]. For extraction of the skeleton, each pixel (*i, j*) in the boundary is assigned a flag value *f* according to the rules given below:

- *f*(*i, j*) = *BAND*, if the pixel belongs to the current position of the moving font.
- *f*(*i, j*) = *INSIDE*, if the pixel is inside the moving font.
- *f*(*i, j*) = *KNOWN*, if the pixel value is outside the moving font.

Each pixel (i, j) in the foreground is assigned a U value. With the above assumptions the following four steps of AFMM are used: initialization, propagation, thresholding, and special boundary points' detection.

Step 1: Initialization

An arbitrary boundary point P, is assigned a value $U = 0$. Starting at P the U value is incremented monotonically along the boundary as illustrated in Fig. 4.9 b). All the boundary pixels are assigned $f(i, j) = KNOWN$ since their U value is known. The pixels inside the boundary are assigned $f(i, j) = INSIDE$ and the pixels outside the boundary are assigned $f(i, j) = KNOWN$.

Step 2: Propagation

Assuming (k, l) is a pixel with known U value, each pixel (i, j) next to the neighbor (k, l) is assigned the value of U using the following algorithm:

If $f(i, j)$ = INSIDE $f(i, j)$ = BAND;

a = average of U over *KNOWN* neighbors of (i, j);

m = min of U over *KNOWN* neighbors of (i, j)

M = max of U over *KNOWN* neighbors of (i, j)

If $((M - m) < 2)$ $U(i, j) = a$;

else $U(i, j) = U(k, l)$;

The evaluation of $f(i, j)$ during propagation is done the same way as in initialization. Fig. 4.9 a) and b) illustrate the initialization of U for a continuous foreground. Similarly, Fig. 4.9 c) and d) illustrate the initialization of U for a

discontinuous foreground. In these figures, the blue pixels represent the boundary, red pixels represent the foreground, and green pixels represent the background. Once the *U* values for the foreground pixels are computed, the skeletal pixels are detected as pixels with sharp discontinuity. More precisely, the pixels having *U* values different from their neighbors by more than a certain threshold value, are taken as skeletal points.

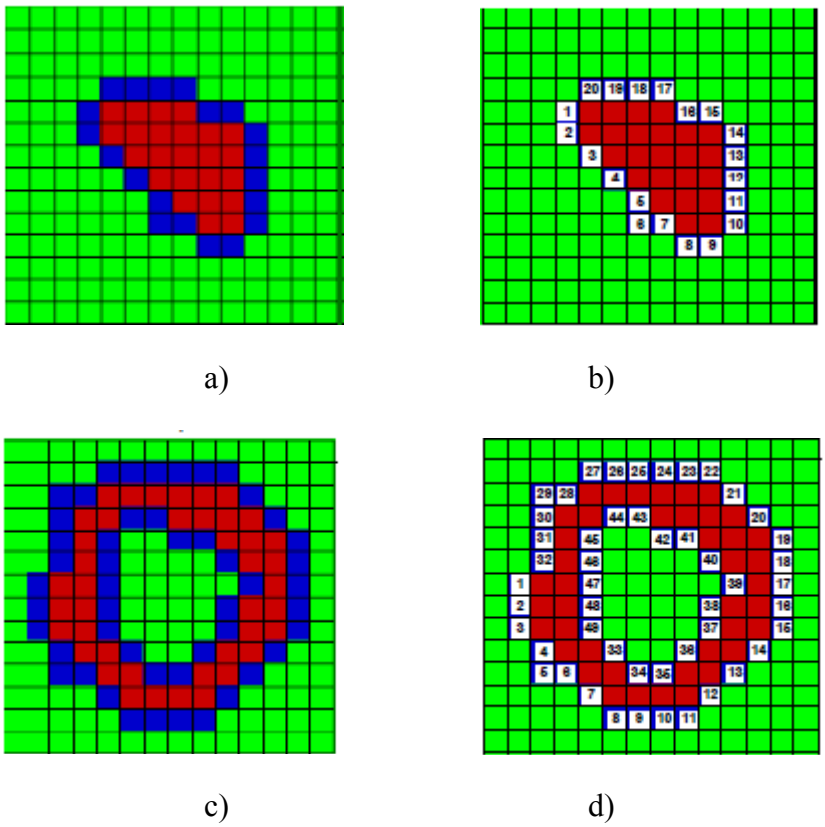

Fig. 4.9: Initialization and propagation of *U* a) a boundary image, b) initialization of *U*, c) moving front, and d) assignment of *U* with the propagating front.

Step 3: Thresholding

For the detection of skeletal points, thresholding is used. As illustrated in Fig. 4.10 a), the maximum distance between any two neighboring pixels is √2, which is the distance between diagonal neighbors. The distance between adjacent neighbors is one. Hence, any value more than √2 could be used as a threshold value for detecting skeletal

points. As shown in Fig. 4.10 b), the pixels with U value of eight and 11, seven and 12, six and 13, four and 15 have a difference of more than two. So if the threshold is set to two, then these points could be detected as skeletal points. The choice of threshold depends on the desired skeleton precision. In this research, the threshold values of 25 and 70 are used.

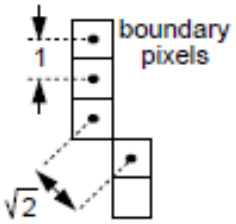

a)

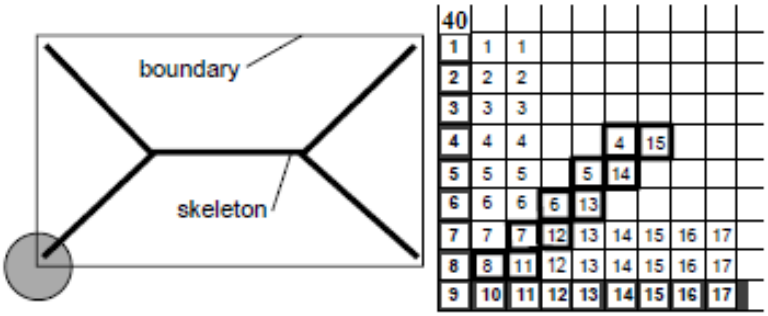

b)

Fig. 4.10: a) The maximum distance to the nearest neighbor pixel and b) illustration of skeletal points.

Step 4: Special boundary points' detection

One of the drawbacks of assigning U values sequentially is shown in Fig. 4.10 b). The boundary point with $U = 1$ and $U = 40$ leads to a skeletal point. However, these points are not the true skeleton points. Fig. 4.11 also illustrates three false skeletal points: 1, 2 and 3. The occurrences of this kind of false skeletal points are removed by calculating the skeleton more than once, each time starting the assignment of U at a

different boundary point. The final skeleton is calculated by taking the intersection of these skeletons.

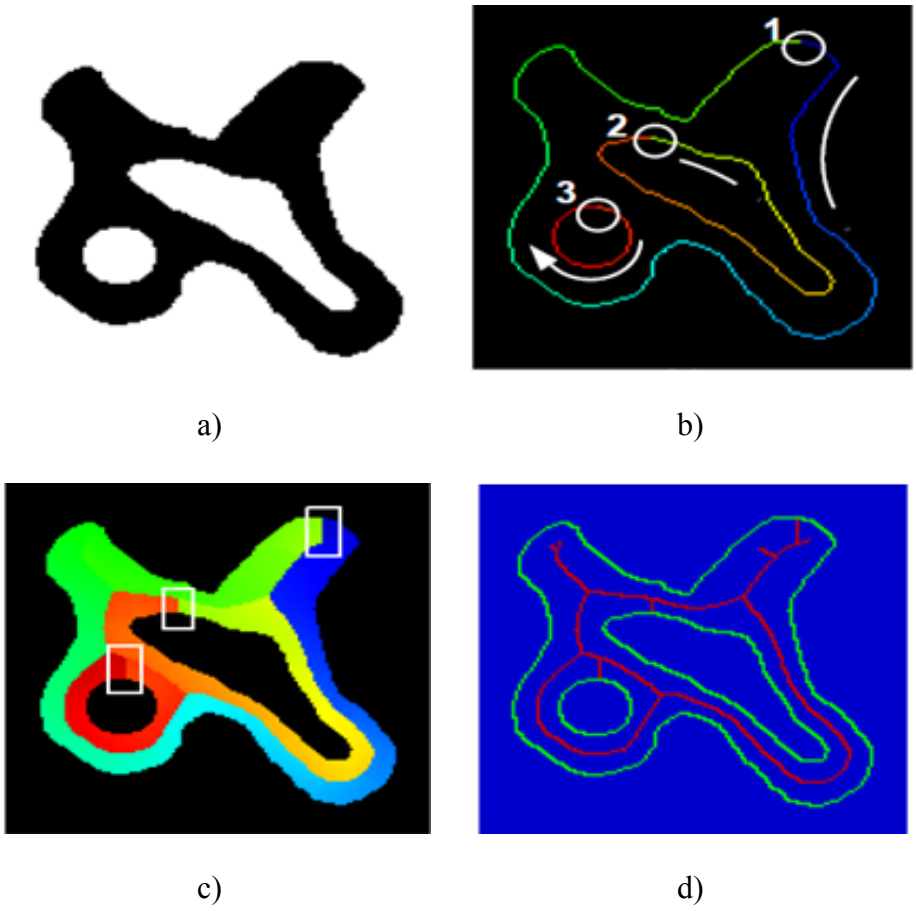

a) b)

c) d)

Fig. 4.11: Treatment of special boundary points: a) original object, b) initial U, c) computed U, d) and the extracted skeleton

In this thesis, the leaf features extracted using the skeleton are the number of junction points and the number of end points. As shown in Fig. 4.12, the points in a skeleton with more than two neighbors are considered as junction points and the points in the skeleton with one neighbor are considered as the skeleton points. The skeleton is calculated using two different threshold levels. A higher threshold level $Thresh_H$ with a value of 70 and a lower threshold level $Thresh_L$ with a value of 25 are used for

skeletonization which results in two different skeletons. From these skeletons the following features are extracted:

Number of end points ($Thresh_H$): The number of junction points in the skeleton extracted using the lower threshold.

Number of junction points ($Thresh_H$): The number of junction points in the skeleton extracted using the higher threshold.

Number of end points ($Thresh_L$): The number of end points in the skeleton extracted using the higher threshold.

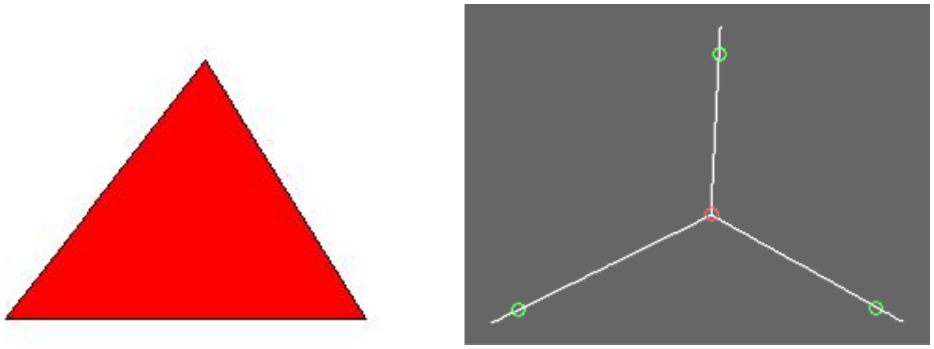

a) b)

Fig. 4.12: a) An arbitrary triangle, b) its skeleton with green circles as the endpoints and red circles as the junction points

4.4. Pattern Classification

After the extraction of the seven features - aspect ratio, isoperimetric ratio, eccentricity, aspect ratio, number of endpoints ($Thresh_L$), number of junctions points ($Thresh_L$) and number of end points ($Thresh_H$) - a training set of 105 leaves images are classified into nine groups using these features. For training, the set of feature values are

used as data points for these images. The range of values for each feature is different; thus, the training data set is normalized using (4.22).

$$u_n^i = \frac{u^i}{\sum_{j=1}^{n} u_j} \tag{4.22}$$

where, u_n^i is a feature in i^{th} data point and n is the total number of data points in the data set.

For pattern classification, K-means clustering [27] is used. K-means clustering aims to cluster a set of d-dimensional observation into k clusters, where each observation or data point belongs to the cluster with the nearest mean. The clustering process is initialized by randomly assigning data points to the k clusters. At each iteration, the data points are placed in the cluster having a center nearest to the data point. The proximity to the centroid is calculated using squared Euclidean distance. After placement of clusters, the cluster centers are recomputed. The algorithm iterates until it converges. Convergence is guaranteed for K-means clustering and is reached when the assignment of data points to the cluster remain constant in two consecutive iterations. In this research, seven features or dimensions are used and some of the features are given a higher weight to produce the best results. The values of the weights used in the study are 1.0, 1.0, 1.0, 1.5, 1.0, 1.15 and 1.95 for isoperimetric quotient, eccentricity, convex hull ratio, number of endpoints using high threshold value, number of junction points using high threshold value, number of endpoints using low threshold value and aspect ratio, respectively. Since nine different leaves shapes as shown in Table 4-1 were studied, a k value of nine is used.

Appendix B contains the information about the number of leaves in each group used in this research. It also contains the name of the plants from which the leaves were extracted.

Table 4-1: Different shapes of leaves used in the classification and their features

Name	Feature
Acicular	Needle shaped as illustrated in Fig. 4.13
Orbicular	Circular as illustrated in Fig. 4.14
Hastate	Triangular with basal loves as illustrated in Fig. 4.15
Elliptical	Oval s as illustrated in Fig. 4.16
Palmate	Human palm shaped as illustrated in Fig. 4.17
Lobed	Lobular with multiples lobes as illustrated in Fig. 4.18
Palmate and doubly serrated	Palmate with doubly serrated margins. Double serrated margins are illustrated in Fig. 4.19
Heart Shaped	Human heart shaped as illustrated in Fig. 4.20
Elliptic and serrated	Elliptic with single serrations. Single serration is illustrated in Fig. 4.21

Fig. 4.13: Acicular leaf

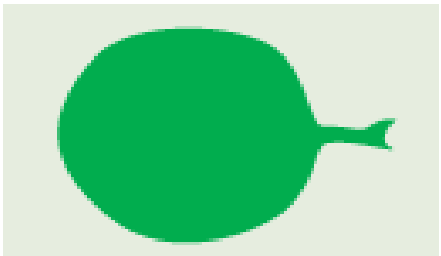

Fig. 4.14: Orbicular leaf

Fig. 4.15: Hastate leaf

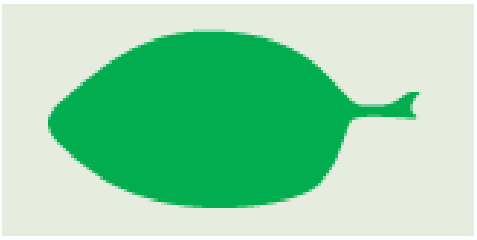

Fig. 4.16: Elliptical leaf

Fig. 4.17: Palmate leaf

Fig. 4.18: Lobed leaf

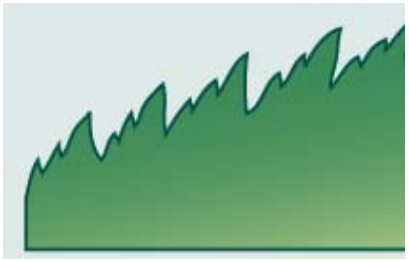

Fig. 4.19: Palmate and doubly serrated leaf's margin

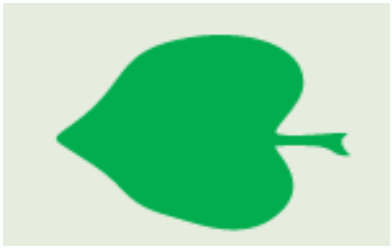

Fig. 4.20: Heart shaped leaf

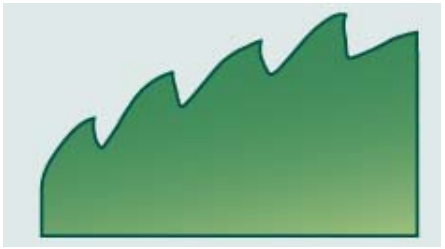

Fig. 4.21: Margin of a elliptic and serrated leaf

4.5. Pattern Recognition

For pattern recognition, a new set of images are tested to validate the classification scheme. These test images contain the leaves of plants already in the database. An application named AppLeClass (Appalachian Leaf Classifier) with a graphical user interface was developed as a part of this thesis for the purpose of testing. The application was developed using MATLAB. Appendix A contains the user manual for this application. Fig. 4.22 shows the snapshot of the graphical user interface (GUI).

As illustrated by the figure, the GUI has six panels. The 'Train Data' panel gives user the flexibility to train a different set of data and 'Training Results' shows the result of the training phase including the centroid for optimized clusters, the number of classes and the normalization coefficients. The 'Test Panel' lets the user select a test image that is shown in 'Test Image' panel. The 'Test Image Features' panel displays the images and values for all the extracted features for the test image. The results are shown in 'Test Results Classification' panel.

4.5.1. Training

A new data set can be trained using this tool. The user has to supply the dataset. There is also an option of loading an already trained data set. A new dataset can be created by using the function "train" of AppLeClass. It further requires the actual training set and the expected cluster identity for each data in the set. The training set should be a matrix of size seven by *n*, where *n* is the number of data points and seven corresponds to the seven features extracted. The expected cluster identity should be provided as a matrix of size one by *n*. The "train" function is defined as:

[*cluster_id, centroids, norm_coeff, stdData*] = train (*training_set*, *num_clusters*)

where, *cluster_id* is the cluster identities given by K-means clustering for each of the data point in the trained dataset *stdData*. *centroids* are the cluster centers and *norm_coeff* is a vector containing normalization coefficients used to normalize the training data set. The inputs to the function, which are the training dataset and the expected number of clusters are provided as *training_set* and *num_clusters*, respectively.

4.5.2. Testing

A new leaf image can be tested against the training set. The images of the test data can be seen in the 'Test Image' panel. The features extracted can also be viewed as images in the 'Test Image features' panel. The tool also displays the five best matched leaves from the existing database along with other pertinent information about the leaf. A web page containing the detailed information about the best matched leaf is also displayed. Detailed description of the tool is provided in Appendix A.

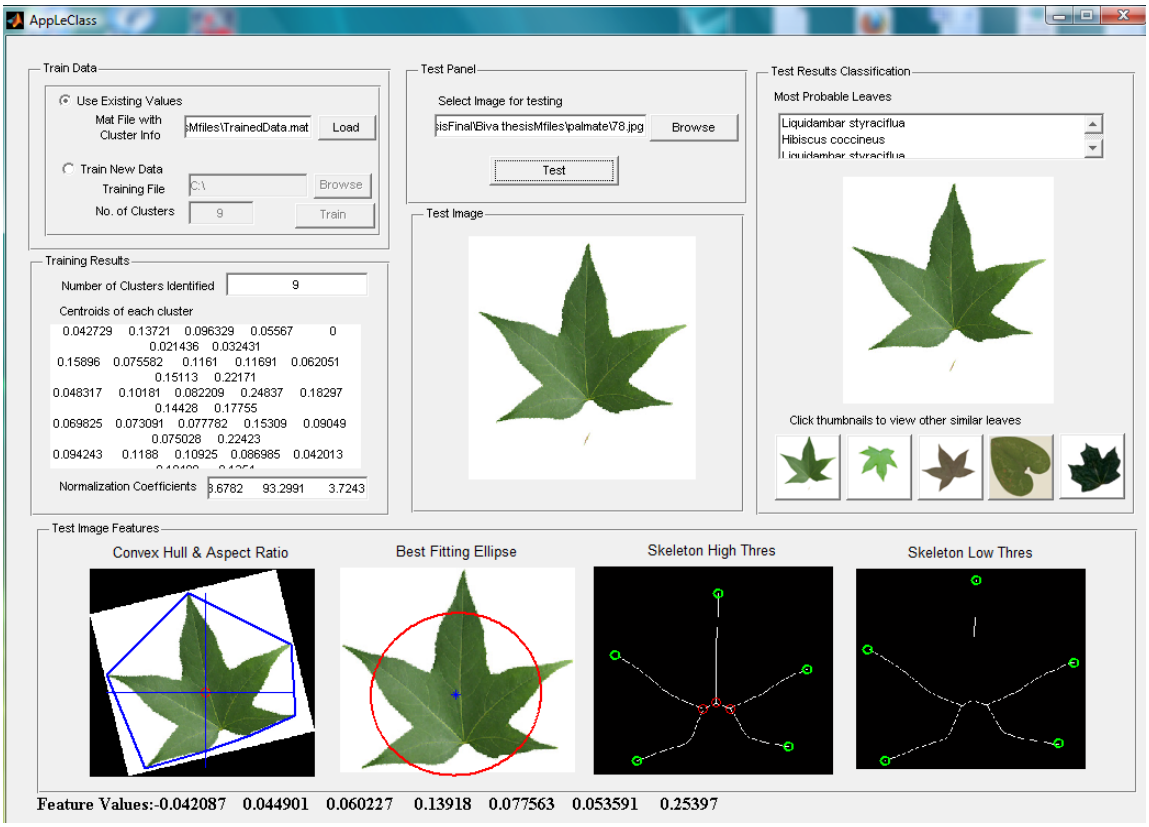

Fig. 4.22: The GUI for AppLeClass

CHAPTER 5: RESULTS

5.1. Image Preprocessing

To get suitable results from the implementation, there are certain protocols that should be followed while testing a leaf image. The protocols are:

- The color of the leaf background must be white or near white.
- The color of the leaf must be different from the color of the background.
- The leaf must not have any white or pale region.
- The leaf image must not be distorted and should not have a petiole attached to it.

Fig. 5.1 illustrates the preprocessing steps of a hastate leaf.

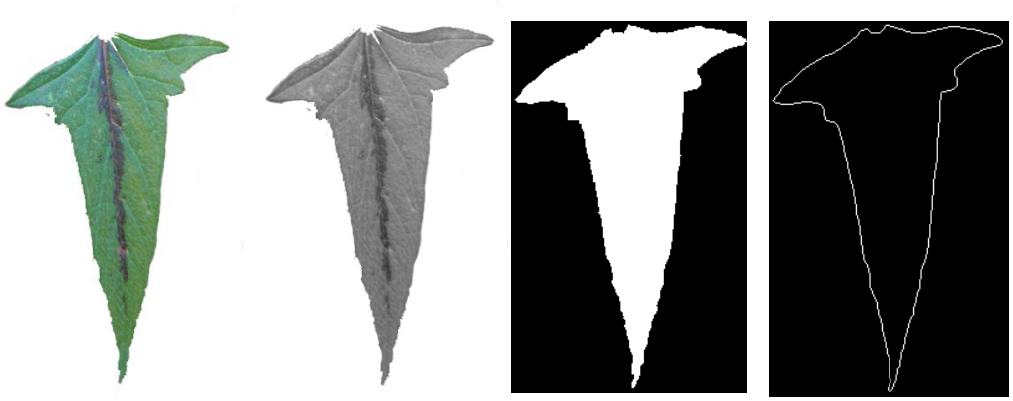

a) b) c) d)

Fig. 5.1: a) A hastate leaf in RGB format, b) conversion to grayscale, c) conversion to binary and d) boundary extraction from the binary image

Fig. 5.2 a) shows a leaf image with uneven coloring. The corresponding grayscale image is shown in Fig. 5.2 b). It is noticeable that some portion of the leaf matches the background color. As thresholding is applied to get the binary image in Fig. 5.2 c), an irregular and distorted shape is formed which does not look like the original leaf. Finally, when the boundary of the leaf is extracted as shown in Fig. 5.2 d) a distorted boundary is obtained. Further analysis is done on this distorted boundary image which results in unexpected values for the features.

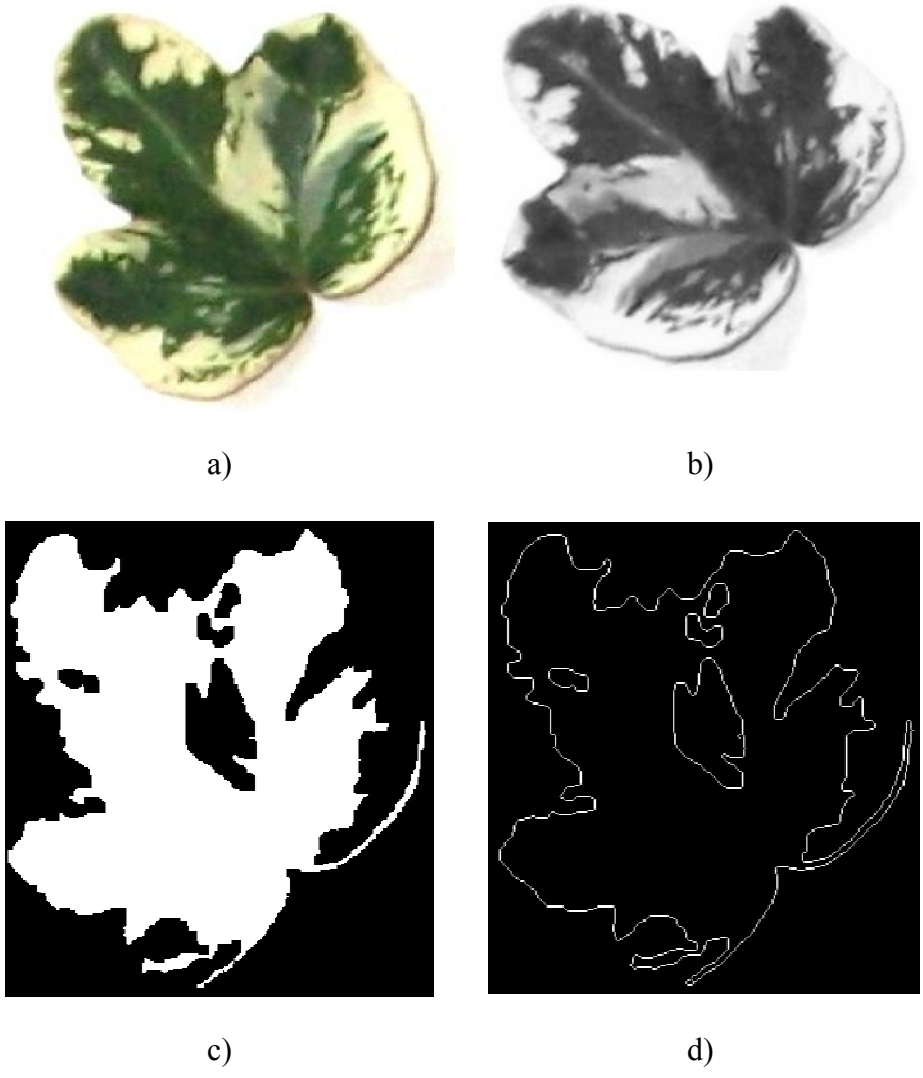

a) b)

c) d)

Fig. 5.2: A leaf with uneven coloring and its boundary detection process

5.2. Convex Hull Ratio

Fig. 5.3 a), b) and c) illustrate the estimation of the convex hull for leaves of acicular, palmate and elliptical shapes, respectively. For a lobed leaf, the area of the leaf surface is less than the area of the convex hull so lobed leaves have comparatively smaller convex hull ratios. In the case where the leaf contained the petiole, an incorrect convex hull is obtained as shown in Fig. 5.4.

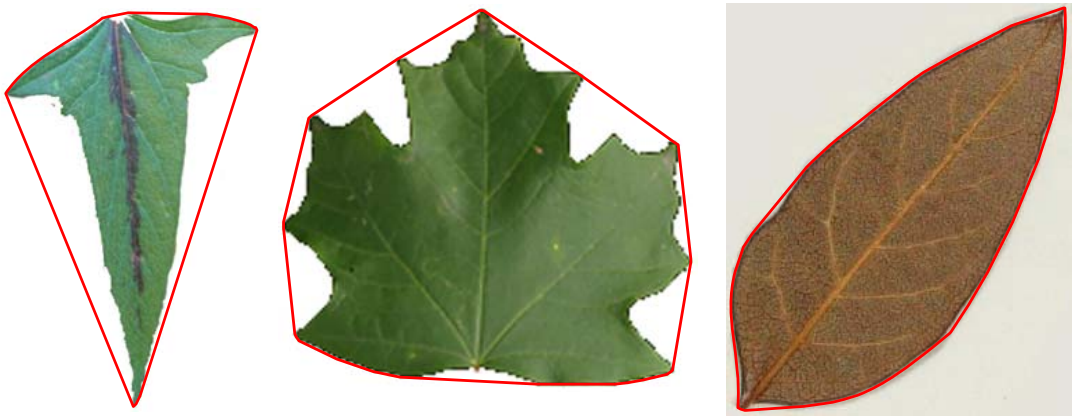

a) b) c)

Fig. 5.3: The area bounded by the red polygon represents the convex hull

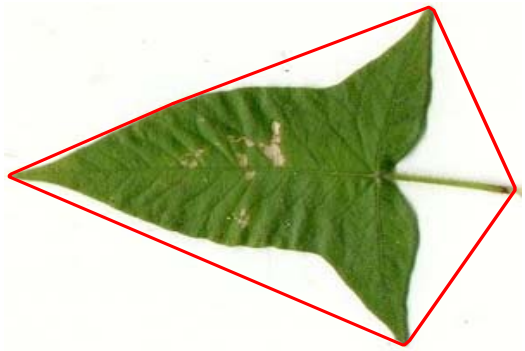

Fig. 5.4: Convex hull being affected by leaf petiole

5.3. Isoperemetric Quotient

Results of isoperemetric quotient extraction shows that leaves with irregular boundaries have smaller isoperemetric quotients which is attributed to the fact that they have larger value for perimeter. Compared to leaves with irregular boundary, the leaves with regular boundary have smaller isoperemetric quotients. There are no errors related to the calculation of isoperimetric quotient except for the case where the leaf boundary is distorted as seen in Fig. 5.2.

5.4. Eccentricity and Aspect Ratio

The best fitting ellipse for acicular, elliptic, and orbicular leaves are shown in Fig. 5.5 and the best fitting ellipse for palmate and hastate leaves are shown in Fig. 5.6. Estimation of the best fitting ellipse is used in extraction of two important features: eccentricity and aspect ratio. Both features determine the shape of the leaf. The best fitting ellipse does not always cover the entire area of the leaf, as seen in the case of palmate and hastate leaves as illustrated in Fig. 5.6.

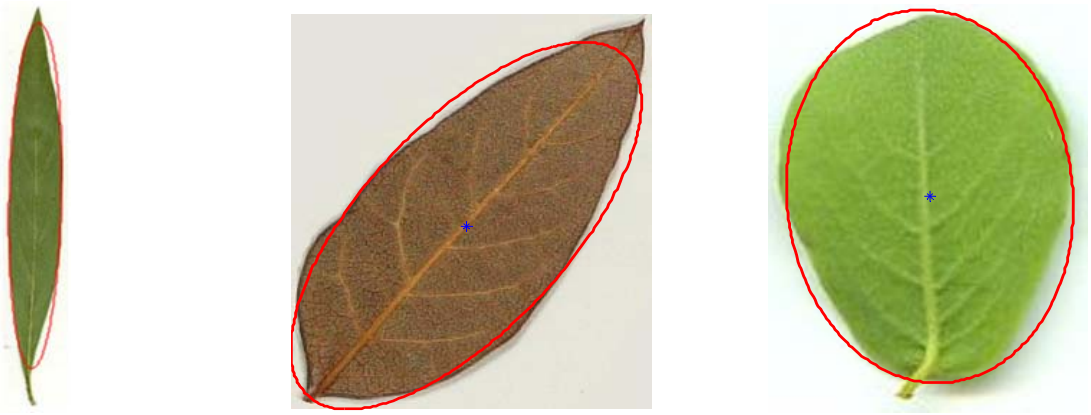

a) b) c)

Fig. 5.5: The best fitting ellipse for a) an acicular leaf b) an elliptic leaf c) an orbicular leaf

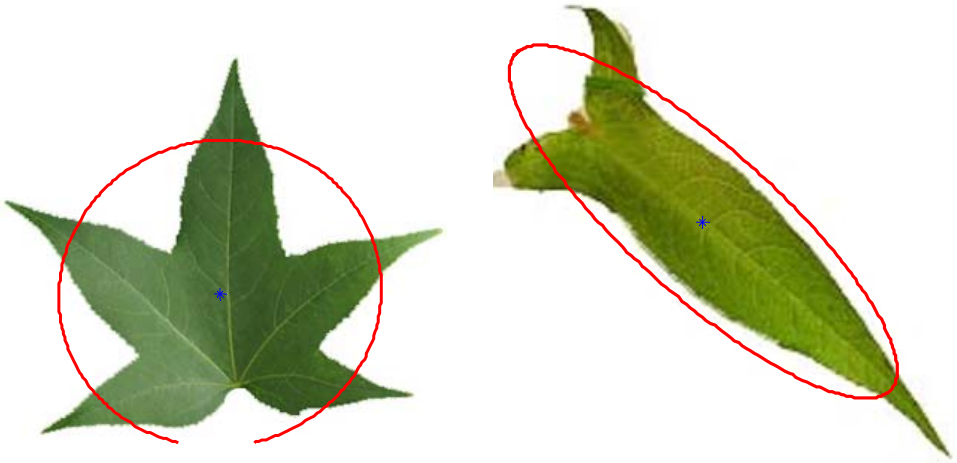

a) b)

Fig. 5.6: The best fitting ellipse for a) a palmate leaf b) a hastate leaf

5.5. Skeleton

The number of end points and the number of junction points obtained from the skeleton calculation using a high threshold value of 70 are used to determine the number of lobes in the leaf. Furthermore, the number of end points extracted from a skeleton using a low threshold value of 25 provides some information on the type of margins of the leaf. Results show that marginated leaves produce a higher number of end points when skeletonized using the lower threshold.

Fig. 5.7 shows the skeletal calculation of an acicular leaf using high and low threshold values. Similarly, Fig. 5.8 shows the skeletal calculation of a hastate leaf. In Fig. 5.7 through Fig. 5.12, green circles represent the end points and red circles represent the junction points. In both acicular and hastate leaves, skeletonization with higher threshold and lower threshold values produce similar skeleton, thus indicating that these leaves are not marginated. On the other hand, as illustrated in Fig. 5.9, if a leaf is

marginated, then it results in a different skeletal structure than that of a similar shaped leaf without margins. The same conclusions can be made by comparing Fig. 5.15 and Fig. 5.16 which show the skeletonization of a palmate leaf and a doubly serrated palmate leaf respectively. It should be noted that the information about serrations of margins is not extractable from the skeleton for lobed leaves. As illustrated in Fig. 5.13, the skeletonization of a serrated lobed leaf at the lower threshold value produces a larger number of endpoints than skeletonization under the higher threshold value. Similar results are obtained when a lobed leaf is skeletonized using high and low threshold values. The results for this case are illustrated in Fig. 5.14. Hence skeletal information is not sufficient for distinguishing a lobed leaf from a serrated lobed leaf; thus, the lobed leaves with serrations are also considered in the lobed group. Skeletal extractions with the high as well as with the low threshold values are shown for a heart-shaped leaf and an orbicular leaf in Fig. 5.11 and Fig. 5.12, respectively.

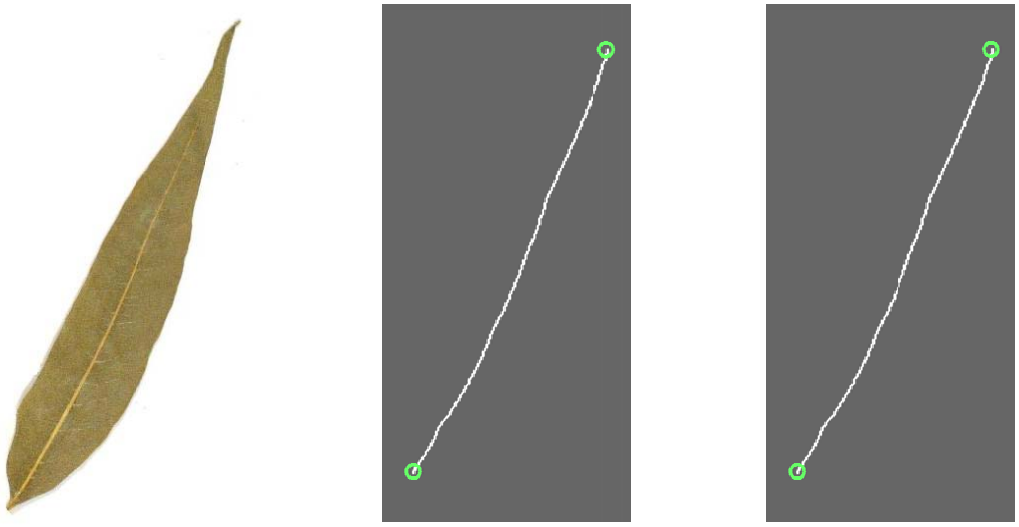

a) b) c)

Fig. 5.7: a) An acicular leaf and its skeletonization in b) high threshold c) low threshold

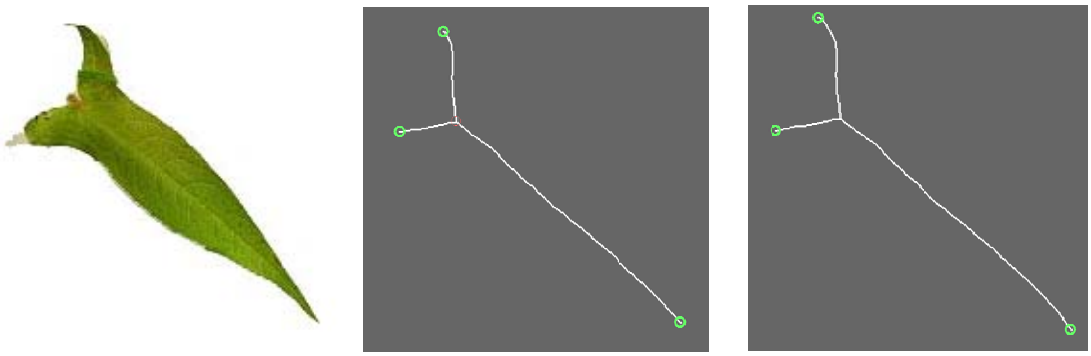

a) b) c)

Fig. 5.8: a) A hastate leaf and its skeletonization in b) high threshold c) low threshold

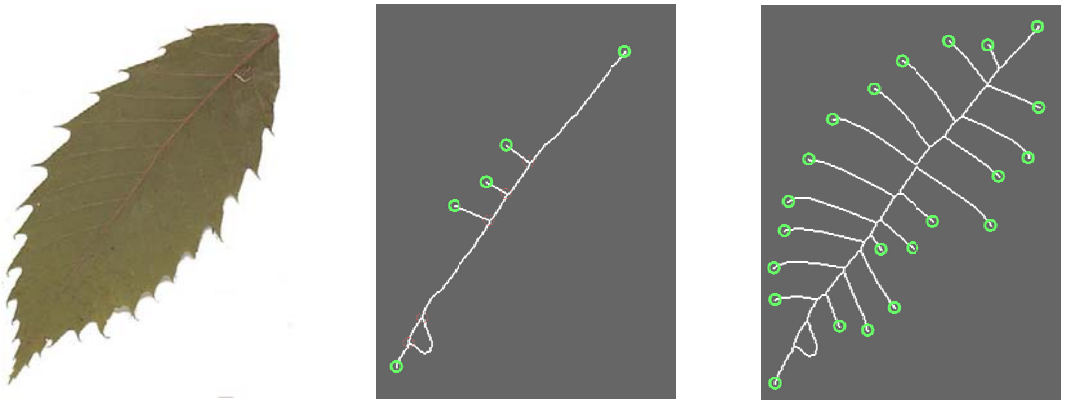

a) b) c)

Fig. 5.9: a) An elliptic and singly serrated leaf, and its skeletonization in b) high threshold c) low threshold

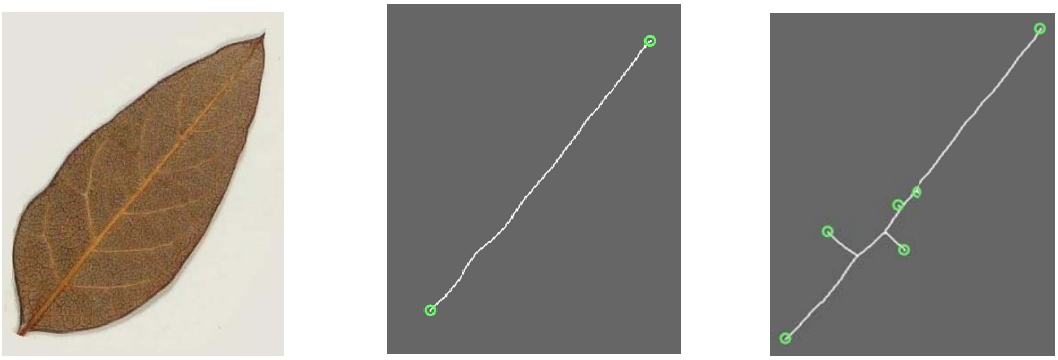

a) b) c)

Fig. 5.10: a) An elliptic leaf and its skeletonization in b) high threshold c) low threshold

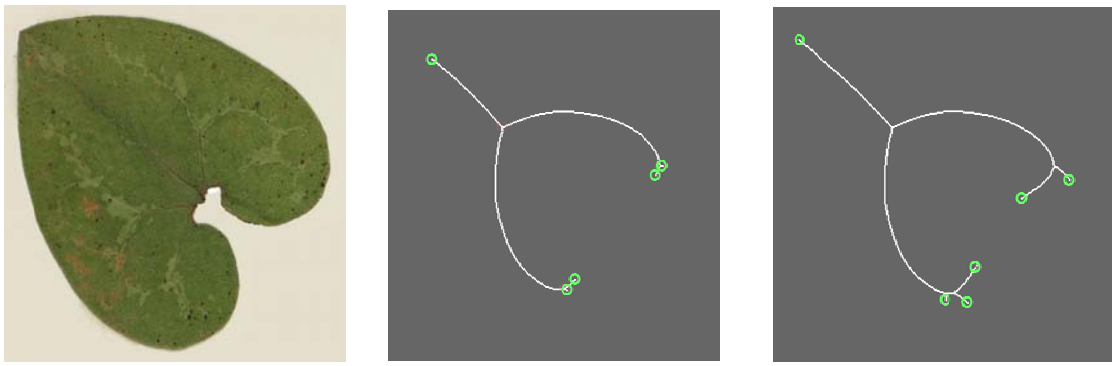

a) b) c)

Fig. 5.11: a) A heart shaped leaf and its skeletonization in b) high threshold c) low threshold

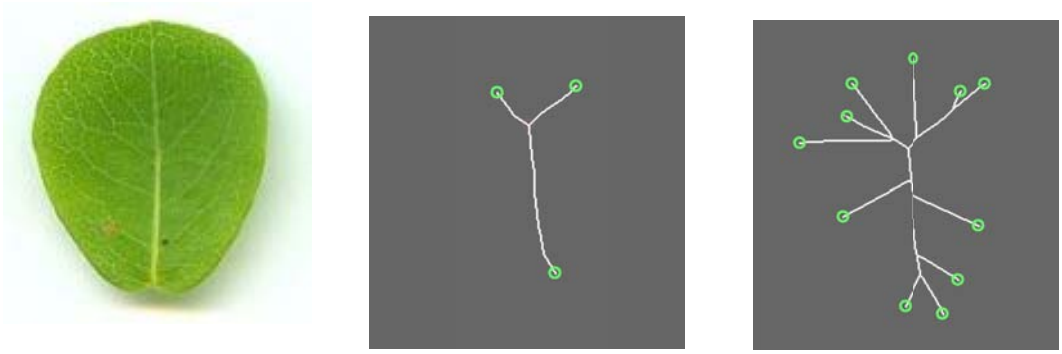

a) b) c)

Fig. 5.12: a) An orbicular leaf and its skeletonization in b) high threshold c) low threshold

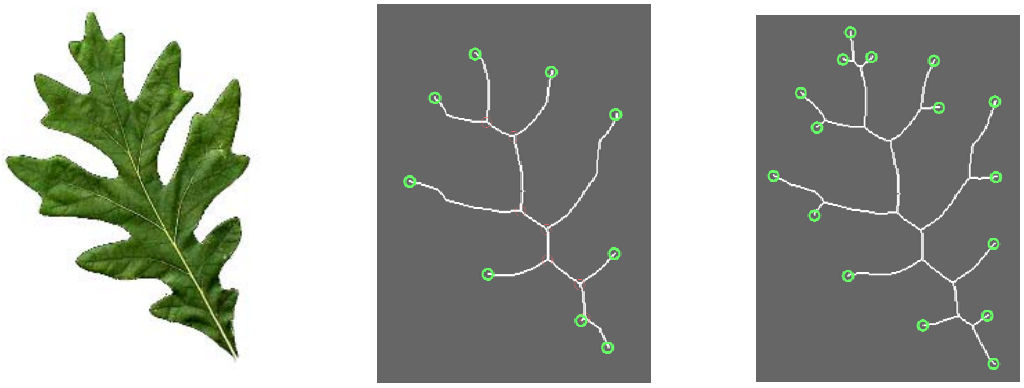

a) b) c)

Fig. 5.13: a) A lobed and serrated leaf, and its skeletonization in b) high threshold c) low threshold

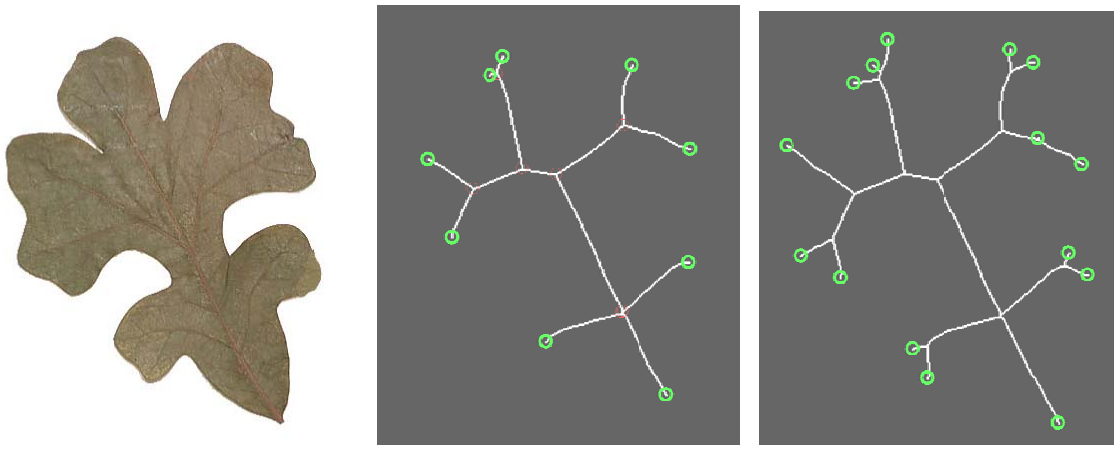

a) b) c)

Fig. 5.14: a) A lobed leaf and its skeletonization in b) high threshold c) low threshold

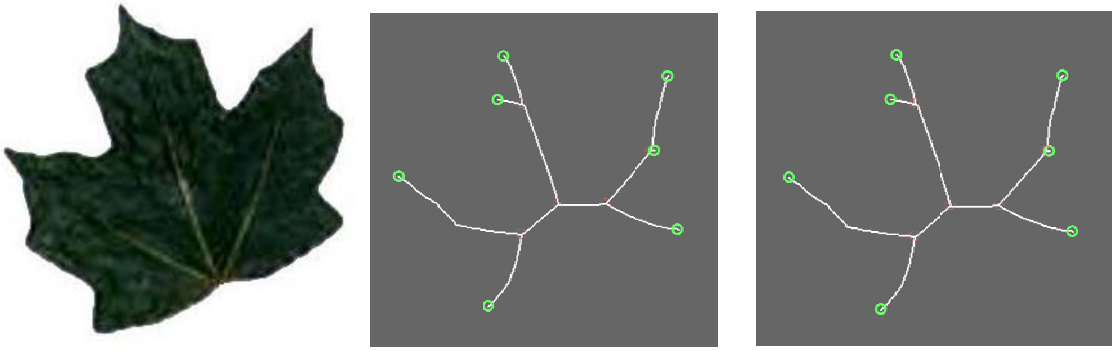

a) b) c)

Fig. 5.15: a) A palmate leaf and its skeletonization in b) high threshold c) low threshold

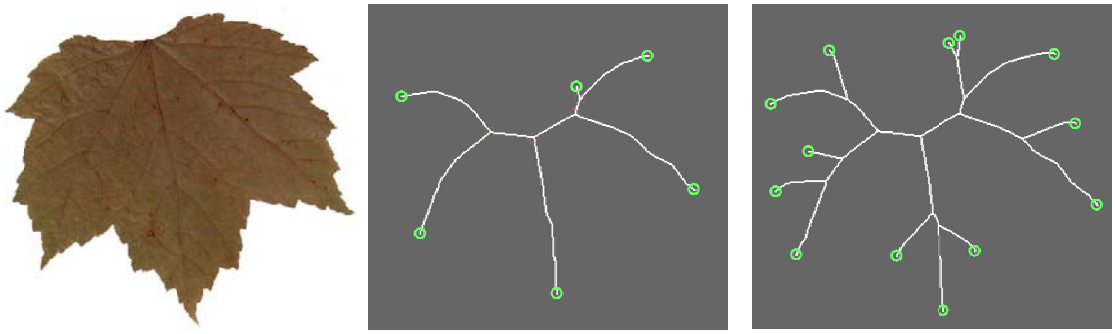

a) b) c)

Fig. 5.16: a) A palmate and doubly serrated leaf, and its skeletonization in b) high threshold c) low threshold

5.6. Classification

In this research, K-means clustering is used to classify 105 leaf images into nine clusters. Hence, 105 data points are formed with each data point having seven dimensions consistent with the seven features extracted (as explained in Chap. 4). Some sample leaf images used in this thesis are presented in Appendix C. Fig. 5.17 shows the distribution of the isoperemetric quotient for the nine clusters. The orbicular leaves had the highest value for isoperemetric quotient as expected. Similarly, the palmate and lobed leaves have low value for isoperemetric quotient which can be explained by the irregularity in their boundaries. The isoperimetric quotient for acicular leaves is also small because of their almost rectangular shape with a very narrow width.

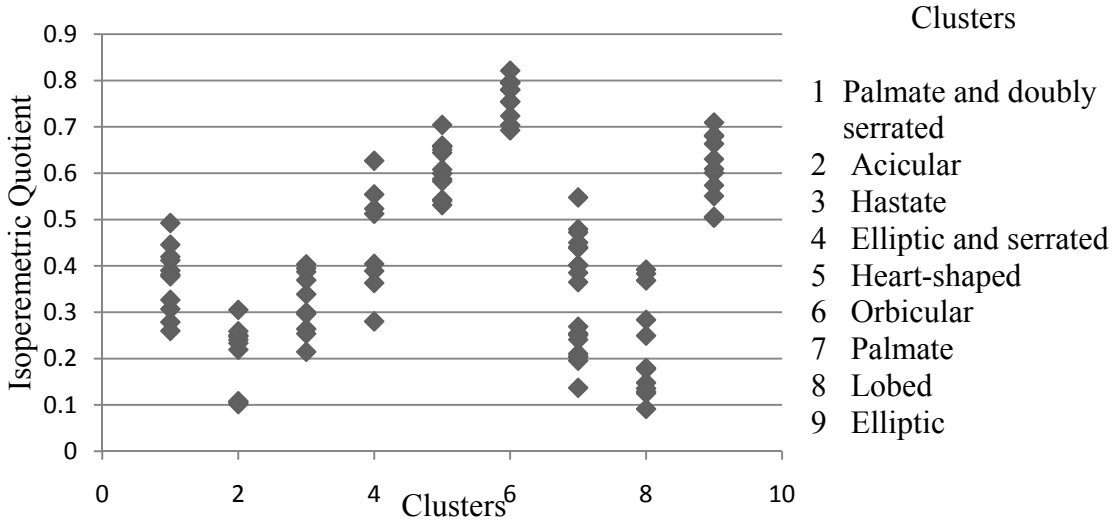

Fig. 5.17: Distribution of isoperimetric quotient

Fig. 5.18 shows the distribution of eccentricity over different clusters. The eccentricity values for palmate and doubly serrated, acicular, and hastate leaves do not overlap with each other. This implies that eccentricity values could be used to differentiate palmate leaves from acicular and hastate leaves. The eccentricity values for

elliptic, and elliptic and serrated, are similar, which is expected. The range was similar for serrated and non-serrated variations of palmate leaves as well.

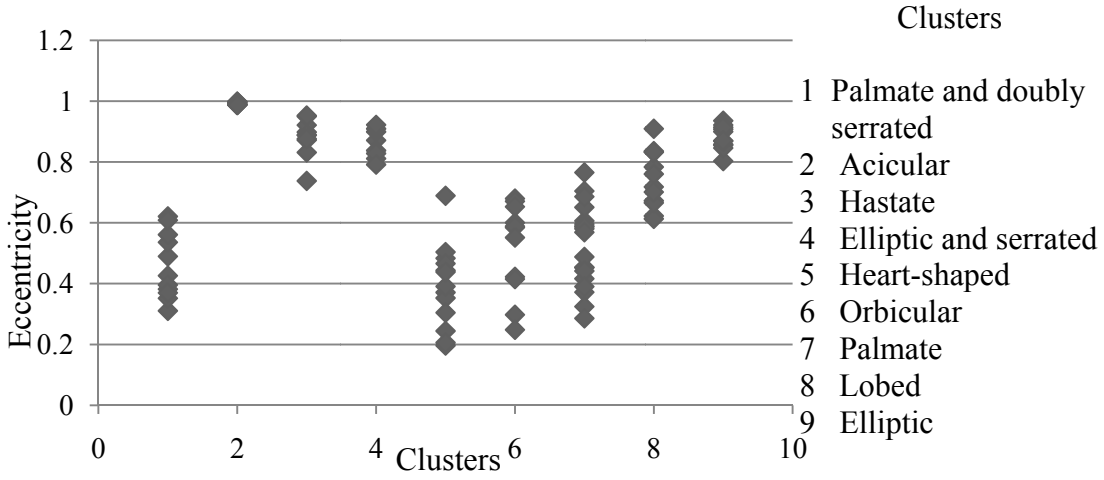

Fig. 5.18: Distribution of eccentricity

Fig. 5.19 shows the distribution of the convex hull ratio over the nine clusters. The elliptic and serrated leaves have very similar values with heart-shaped leaves. Also, this is the case with orbicular leaves and elliptic leaves. However, these two categories of leaves have values that are non-overlapping and thus could be classified easily.

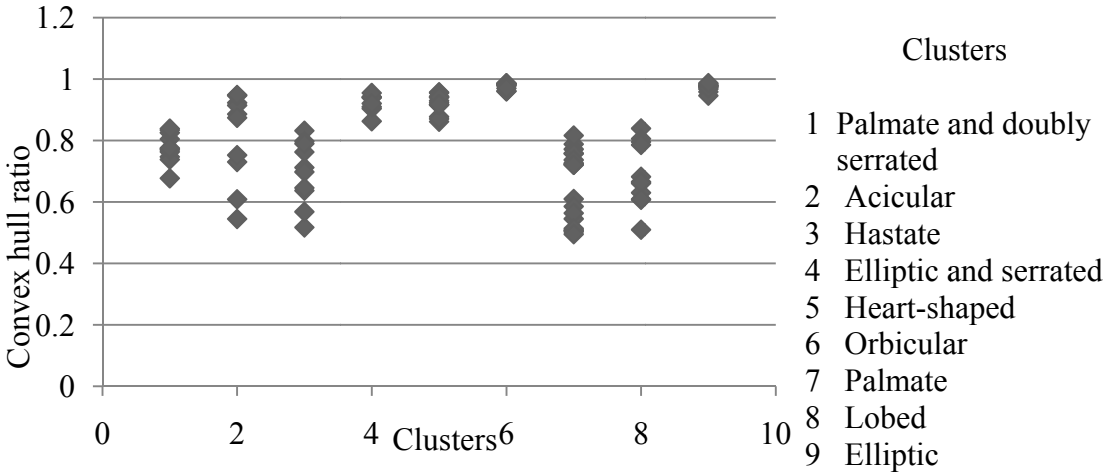

Fig. 5.19: Distribution of convex hull ratio

Fig. 5.20 shows the distribution of aspect ratio over different clusters. Acicular leaves have the lowest values for aspect ratio as expected. Also, hastate leaves and elliptical leaves have comparatively low value for aspect ratio.The elongated triangle-like shape of hastate leaves contributes to their low aspect ratio.

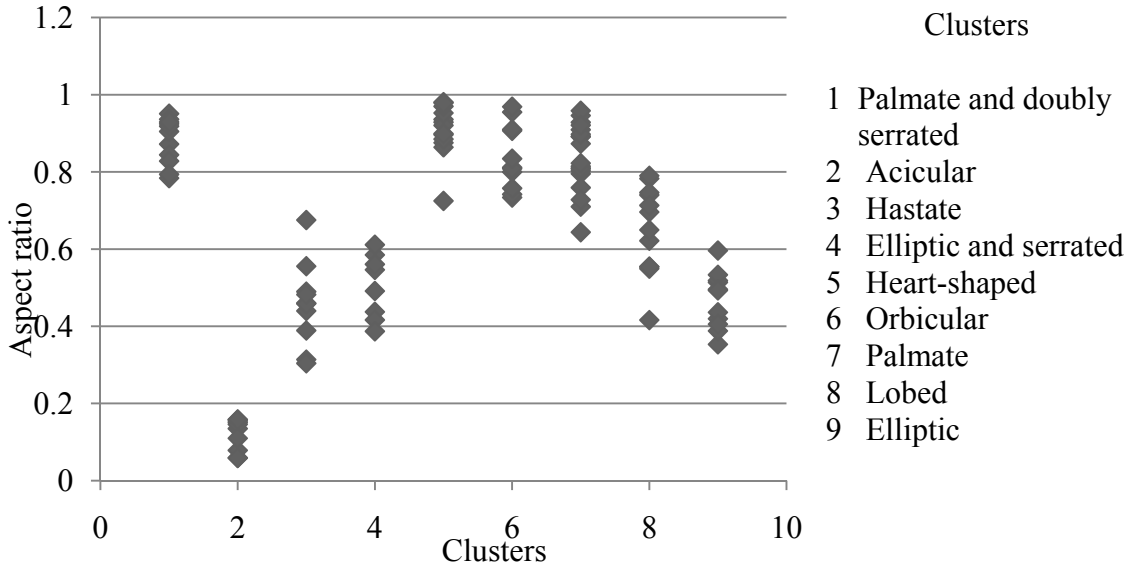

Fig. 5.20: Distribution of aspect ratio

Fig. 5.21 shows the distribution of endpoints across the clusters. These endpoints are estimated using the high threshold value in skeletonization. Acicular, as well as elliptic leaves yield two end points. Heart shaped leaves have 2-6 endpoints, while serrated elliptic leaves have more end points than elliptic leaves due to the serrations; similarly, the skeletons of palmate and doubly-serrated leaves have a higher number of end points than palmate leaves.

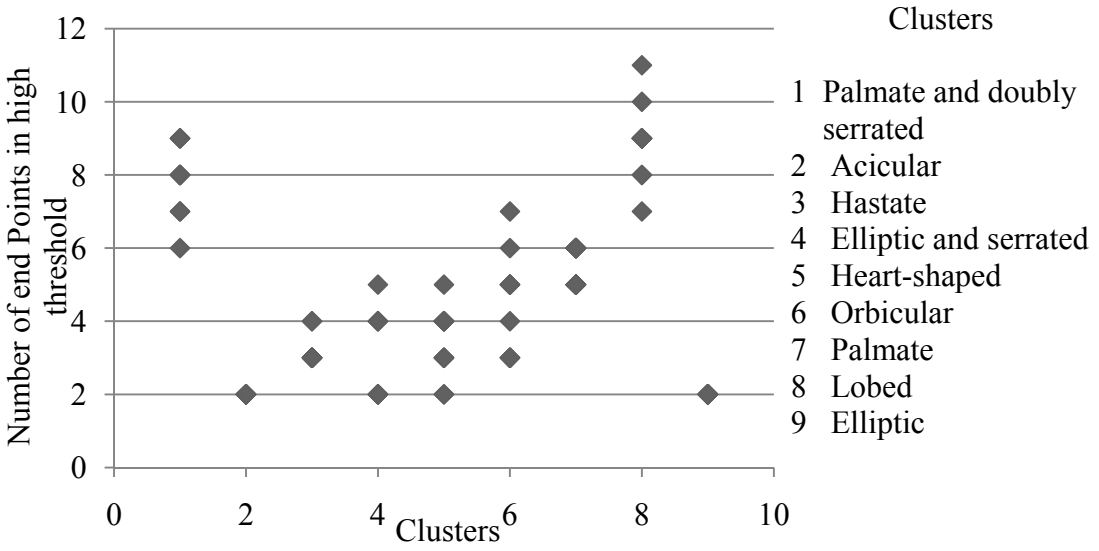

Fig. 5.21: Distribution of number of end points estimated from high threshold skeletonization

Fig. 5.22 shows the distribution of junction points across the clusters. The junction points are estimated using the high threshold value during skeletonization. Elliptic, ellliptic and serrated, and acicular leaves do not have any junction points.

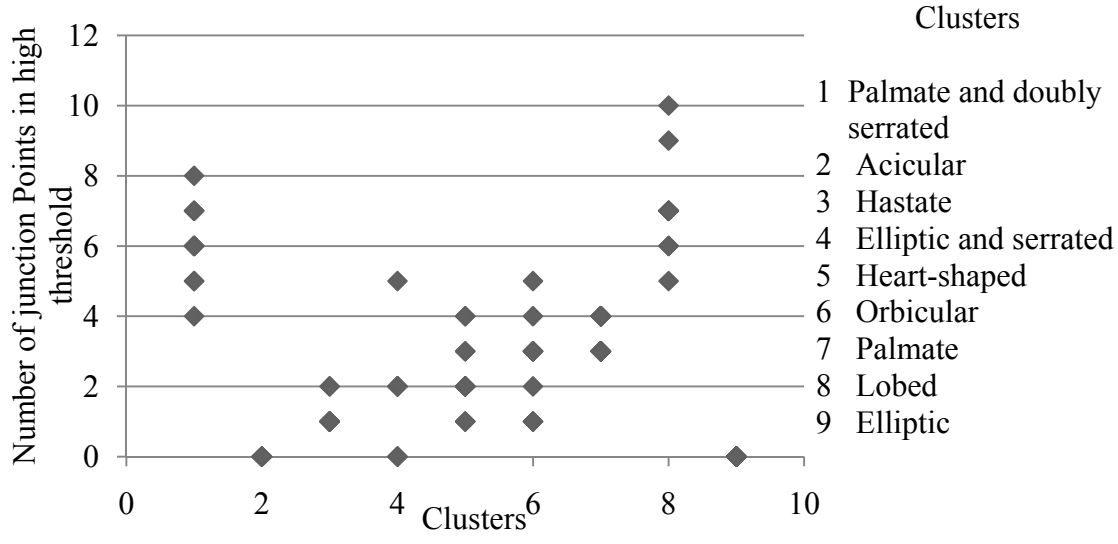

Fig. 5.22: Distribution of number of junction points estimated from high threshold skeletonization

Fig. 5.23 shows the distribution of the number of end points across the clusters. These end points are estimated using the low threshold value during skeletonization. Comparing Fig. 5.21 and Fig. 5.23, serrated leaves have a larger number of end points when using the low threshold value than while using the high threshold value during skeletonization. This leads to the detection of serration.

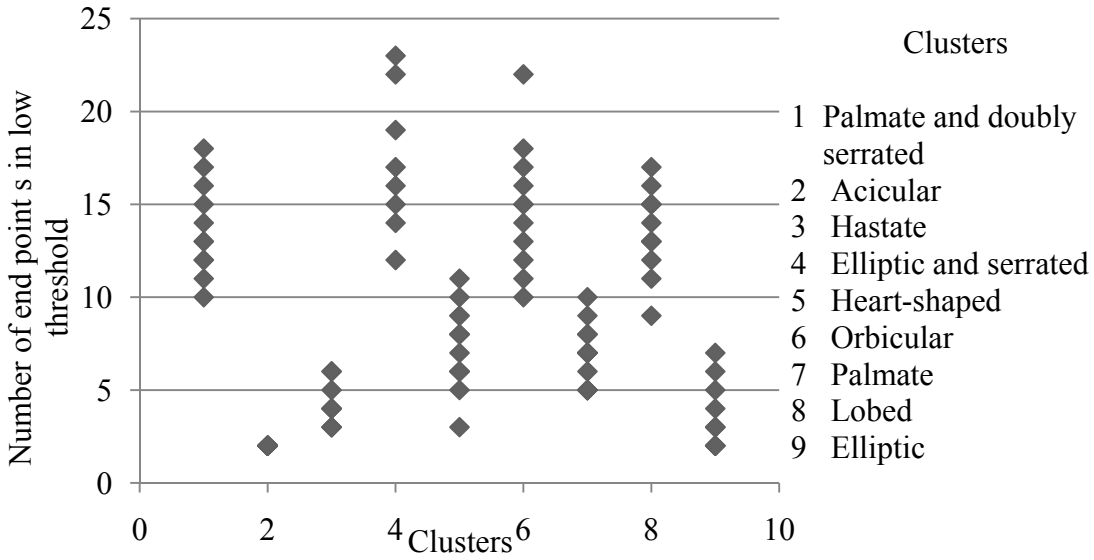

Fig. 5.23: Distribution of number of end points estimated from low threshold skeletonization

Table 5-1 shows the accuracy of the clustering algorithm. Accuracy for each cluster as well as the overall acurracy of the developed classification scheme is illustrated. In this table, the overall accuracy obtained from this implemenation is 97.14% on 105 leaves belonging to nine clusters.

Table 5-1: Results of clustering algorithm

Cluster	Number of data points	True positive	False positive	Accuracy
Palmate and doubly serrated	11	9	2	81.81%
Acicular	10	10	0	100.00%
Hastate	10	10	0	110.00%
Elliptic and serrated	8	8	0	100.00%
Chordate (Heart-Shaped)	13	13	0	100.00%
Orbicular	11	10	1	90.91%
Palmate	19	19	0	100.00%
Lobed	12	12	0	100.00%
Elliptical	11	11	0	100.00%
Total	105	102	3	97.14%

5.7. Recognition

AppLeClass is used in this research for testing new leaf images which displays the five best matches of the target leaf. The test image is examined on the training set and the three nearest clusters are evaluated. From the closest cluster, three best matches are presented. Similarly, from each of the second and third closest clusters, one best match is presented. The result of the test is presented in Table 5-2. As shown in this table, the accuracy of leaf class recognition is 100%. The accuracy of leaf species recognition is 89.65%. A correct identification of leaf species implies that the algorithm not only classifies the new leaf as falling under a certain class (e.g. acicular) but also identifies the exact plant to which the leaf belongs.

Table 5-2: Recognition results for the test data set

Leaf name	Species match	Class match
Liriodendron tulipifera	Yes	yes
Acer rubrum	Yes	yes
Acer rubrum	Yes	yes
Lysimachia lanceolata	Yes	yes
Palafoxia callosa	Yes	yes
Quercos phellos	Yes	yes
Vinca major	Yes	yes
Apocynum cannabinum	Yes	yes
Apocynum medium	Yes	yes
Andrachne phyllanthoides	Yes	yes
Quercos Velutina	Yes	yes
Castanea Dentata	Yes	yes
Fagus grandifolia	Yes	yes
Hexastylis contracta	Yes	yes
Hexastylis naniflora	Yes	yes
Hibiscus Coccineus	Yes	yes
Hexastylis virginica	**No**	yes
Liquidambar styraciflua	Yes	yes
Lonicera Implexa	**No**	yes
Liriodendron tulipifera	Yes	yes
Phacelia purshii	Yes	yes
Populus_tremuloides	**No**	yes
Quercus alba	Yes	yes
Quercus rubra	Yes	yes
Quercus stellata	Yes	yes
Quercus velutina	Yes	yes
Saintpaulia grotei	Yes	yes
Saintpaulia Robertson	Yes	yes
Senecio Obvatus	Yes	yes

CHAPTER 6: Conclusions and Future Recommendations

6.1. Conclusion

In this research, various features related to the shape of the leaves were studied and the most appropriate features were used for leaf image-based plant classification. The features selected in this automated plant identification were: 1) isoperimetric quotient, 2) convex hull ratio, 3) aspect ratio, 4) eccentricity and 5) number of endpoints and junction points in the skeleton of the leaf. These features were vital in identifying leaf shapes, number of lobes and margin types. Leaves of nine classes were used and a classifier was implemented and tested using 105 leaves of 38 different species.

6.1.1. Isoperemetric Quotient

The isoperemetric quotient was obtained by calculating the area and the perimeter of the leaf. Area was calculated by counting the number of pixels in the foreground. Similarly, perimeter was calculated by counting the number of pixels in the boundary of the leaf. From the results of this research, observations were made that the isoperemetric quotient is greater for circular leaves with regular margins. Elongated leaves and leaves with irregular margins had a comparatively lower isoperemetric quotient than other leaves.

6.1.2. Eccentricity and Aspect Ratio

For calculation of eccentricity, the best fitting ellipse was estimated using the central moment of the leaf shape, which is a region-based method. A region-based method was used instead of a boundary-based method because the region based method was not sensitive to the irregularities in boundary of a shape. From the best fit ellipse, the aspect ratio was also calculated. The results of the research show that eccentricity and aspect ratio together were important in differentiating elongated leaves from circular leaves. Aspect ratio and eccentricity were not sensitive to the margin information.

6.1.3. Convex Hull Ratio

The convex hull was calculated using Andrew's monotone chain algorithm. Andrew's monotone chain algorithm worst case scenario performance was equal to the regular Graham's scan's performance.

The results of this research showed that leaves without lobes and leaves with regular boundaries have a lower convex hull ratio than leaves with irregular boundaries and leaves with lobes.

6.1.4. Skeleton

The skeleton was calculated using an augmented fast marching method. The results from the skeleton extracted in higher threshold were important in distinguishing the number of lobes in a leaf. Elliptic leaves had two endpoints, and heart-shaped leaves had three endpoints and one junction point. The number of endpoint and junction points increased with the increase in the number of lobes. Similarly, skeleton extracted in lower

threshold gave some information about the boundary margins. More endpoints were detected in palmate leaves with serrations than those in palmate leaves when skeletonized using lower threshold.

6.1.5. Summary

All the traninng and testing was done using the application AppLeClass which was developed as a part of the research. The tool has all the functionalities required for testing and training. AppLeClass displays the features extracted for an image and displays the five best matches of the target leaf. Hence, calculation of efficiency and error was simplified and studying a pattern in the erroneous cases was convenient.

The results for the training set of images used in this research indicates an accuracy of 97.14% for the classification algorithm. Results from the test data set show that the classification algorithm identifies the class of these leaves 100% of the time whereas the accuracy in identifying the exact species of the leaf was 89.65%.

The errors in identification mostly corresponded to two inaccuracies during the image processing stage. The first incurracy was in identifying the correct type of margins. The error propagated to the feature extraction phase. This kind of error was prominent in leaves with very subtle margins. The second incurracy was seen in extracting the number of lobes using the skeleton. The skeleton approach was found to be sensitive to leaf curvature, thus sometimes giving erroneous output for lobe identification.

6.2. Future Recommendations

The research can be improved using a larger training set with other leaf shapes. In the data collection phase, leaves were cut from a herbarium specimen manually and the

noise in the leaf background was removed manually. These processes can be automated for future analyses.

The features used in this research were not robust for leaves with irregular margins. Further analyses can be conducted to improve the current feature extraction process and to include additional features to make the agorithm robust for all kinds of leaf.

BIBLIOGRAPHY

[1] W. E. Snyder and H Qi, *Machine Vision*, Cambridge, MA: Cambridge university press, 2004.

[2] M. J. Dallwitz (1980). *A general system for coding taxonomic description* [online]. vol. 29. Available:http://delta-intkey.com

[3] D. Warren, "Automated leaf shape description for variety testing in chrysanthemums," in *Proc. 6th Int. Conf. Image Process. and Its Applicat.,* Duplin, Ireland, 1997.

[4] Z. Miao *et al*., "An oopr-based rose variety recognition system," *Engineering Applications of Artificial Intelligence,* vol. 19, issue 5, Amsterdam, Elsevier, 2006, pp. 78-101.

[5] B. C. Heymans *et al*., "A neural network for Opuntia leaf-form recognition," *IJCNN*, vol. 3, pp. 2116-2121, 1991.

[6] T. Satioh and T. Kaneko, "Automatic Recognition of Wild Flowers", *ICPR*, vol. 2, pp. 2507-2510, 2000.

[7] Y. Li *et al*., "A leaf vein extraction method based on snakes technique," in *Proc. Neural Networks and Brain Int. Conf.*, Beijing, China, 2005.

[8] M. Kass *et al*., "Snakes: active contour models," in *Int. Journal of Computer Vision*, vol. 1, Boston, MA: Kluwer Academic Publishers, 1987, pp. 321–331.

[9] H. Fu and Z. Chi, "Combined thresholding and neural network approach for vein pattern extraction from leaf images," *IEE Proc. Vision, Image and Signal Process.*, vol. 153, issue 6, 2006, pp. 881-892.

[10] H. Qi and J. G. Yang, "Saw tooth feature extraction of leaf edge based on support vector machine," *ICMLC*, vol. 5, pp. 3039-3044, 2003.

[11] Y. Nam *et al*., "Elis: An efficient leaf image retrieval system", in *Proc. Advances in Pattern Recognition Int. Conf.*, Kolkata, India, 2005.

[12] H. Fu and J. Chi, "A two-stage approach for leaf vein extraction," *ICNNSP*, vol. 1, pp. 208-211, 2003.

[13] X. Gu *et al*.,. Wang, "Leaf recognition based on the combination of wavelet transform and gaussian interpolation," *ICIS*, vol. 3644/2005, pp. 253-262, 2005.

[14] J. X. Du *et al*., "Leaf shape based plant species recognition," *Applied Mathematics and Computation*, vol. 185, issue 2, Amsterdam, Elsevier, 2007, pp. 883-893.

[15] H. Fu *et al*., "Machine learning techniques for ontology-based leaf classification," *ICARCV*, vol. 1, pp681-686, 2004.

[16] X. F. Wang *et al*., "Recognition of leaf images based on shape features using a hypersphere classifier," *ICIC*, vol. 3644/2005, pp. 87-96, 2005.

[17] S. Wu *et al*., "A Leaf Recognition Algorithm for Plant Classification Using Probabilistic Neural Network," in *Proc. Signal Process. and Inform. Technology, IEEE Int. Symp*., Cairo, Egypt, 2007.

[18] A. Talea, "An augmented fast marching method for computing skeleton and centerlines," in *IEEE TCVG Sym. Visualization*, Barcelona, 2002.

[19] H. Blum, "A transformation for extracting new descriptors of shape," in *Models for the Perception of Speech and Visual Form*, Cambridge, MA: MIT Press, 1967, pp. 360-380.

[20] H. Blum and R. N. Nagel, "Shape description using weighted symmetric axis features," in *Pattern Recognition,* vol. 10, issue 3, Amsterdam, Elsevier, 1978, pp. 167-180.

[21] R. L. Ogniewicz, "Automatic Medial Axis Pruning by Mapping Characteristics of Boundaries Evolving under the Euclidean Geometric Heat Flow onto Voronoi Skeletons," Harvard Robotics Lab., Cambridge, MA, Tech. Rep. 95-4, 1995.

[22] J. A. Sethian, "A Fast Marching Level Set Method for Monotonically Advancing Fronts," *PNAS*, vol. 40, pp. 1528-1538, 1995.

[23] S. Wu and A. Amin, "Automatic Thresholding of Gray-level Using Multi-stage approach," *IEEE Trans Syst Man Cybern*, vol. 9, issue 1, pp. 62-66, 1979.

[24] J. Canny, "A Computational Approach to Edge Detection," *IEEE Trans. Pattern Anal. Mach. Intell.*, vol. 8, issue 6, pp. 679-698, 1986.

[25] A. M. Andrew, "Another Efficient Algorithm for Convex Hulls in Two Dimensions," *Inform. Process. Lett*., vol. 9, issue 5, pp. 216-219, 1979.

[26] R. L. Graham, "An Efficient Algorithm for Determining the Convex Hull of a Finite Planar Set," *Inform. Process. Lett*., vol. 1, issue 4, Amsterdam, Elsevier, 1996, pp. 132-133.

[27] J. B. MacQueen, "Some methods for classification and Analysis Multivariate Observations," in *Proc. 5th Berkeley Symp. Math. Stat. and Probability*, Berkley, CA, 1967.

APPENDIX A

User Manual for AppLeClass

The GUI

Interactive Panels as shown in* Fig. A.1*:

- Train Data
- Training results
- Test Image
- Test Panel
- Test Image features
- Test results Classification

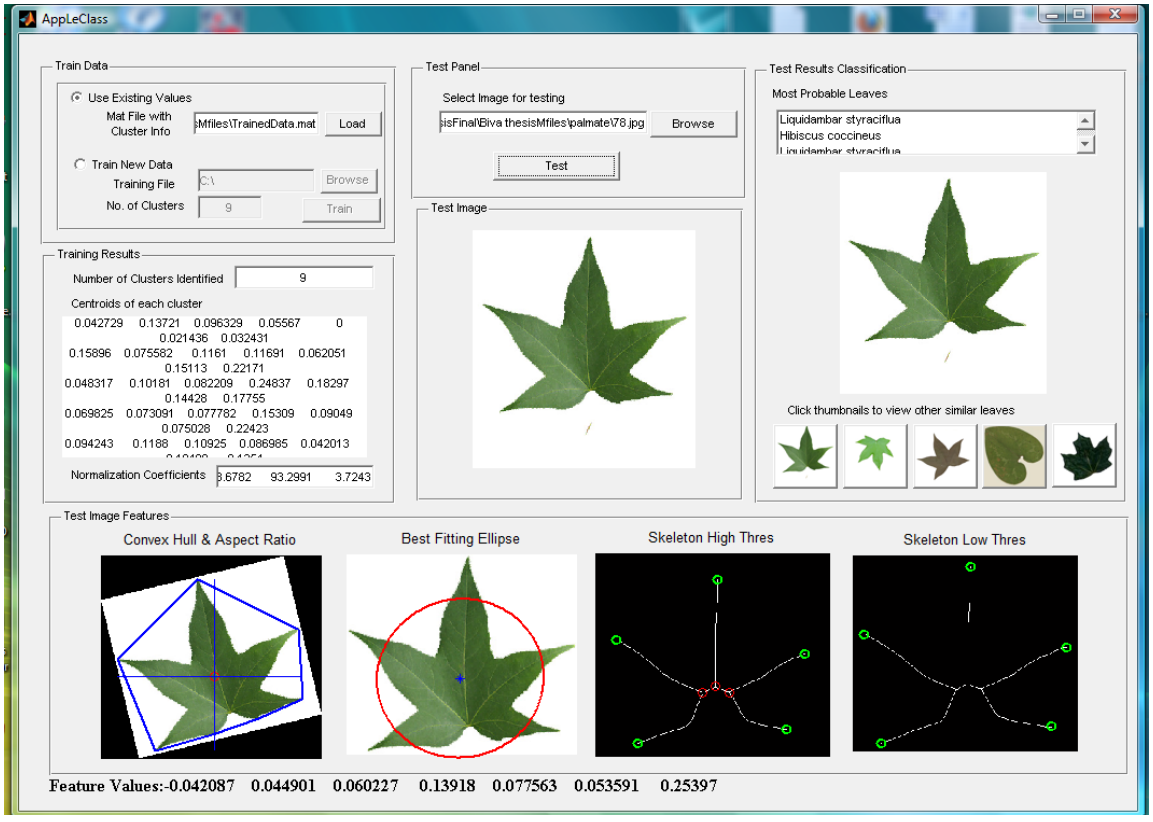

Fig. A.1: The GUI for AppLeClass

Train Data

Interactions as shown in* Fig. A.2*:

Load the already trained data: The radio button 'Use Existing Values' must be enabled and load button pushed.

Train new data set: The radio button 'Train New Data' must be enabled and then the browse button can be used to browse the input data set to be trained.

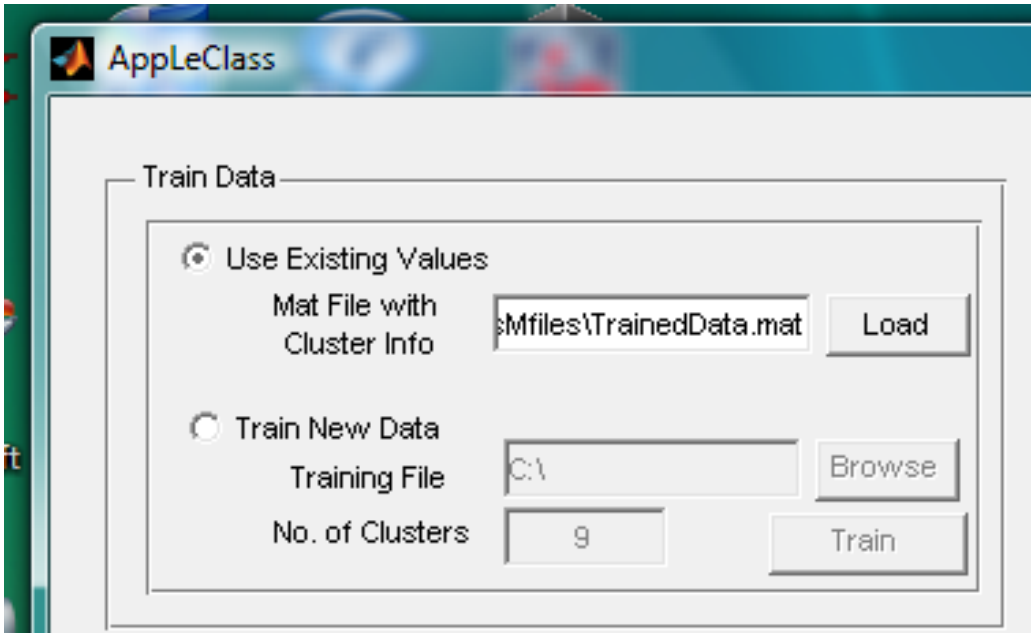

Fig. A.2: The Train Data panel for AppLeClass

Training Results

Interactions as shown in* Fig. A.3*:

Number of clusters identified: The 'Number of Clusters Identified' text box shows the total number of cluster detected.

Centroids of each cluster: The 'Centroids of each cluster' text box shows the centers of the clusters detected.

Normalization coefficients: The 'Normalization Coefficients' text box shows the normalization coefficients used.

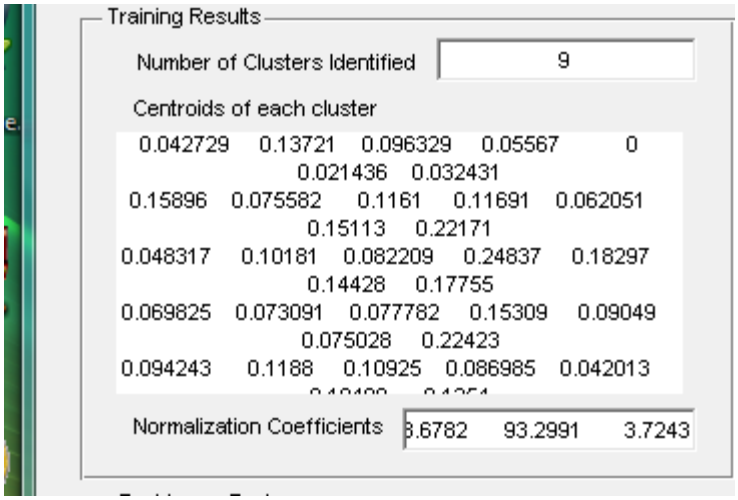

Fig. A.3: The Training Results panel for AppLeClass

Test Panel and Test Image

Interactions as shown in* Fig. A.4*:

Image selection: The 'Select Image for testing' browse button can be used to browse the test image.

Test image display: The 'Test Image' panel shows the test image browsed.

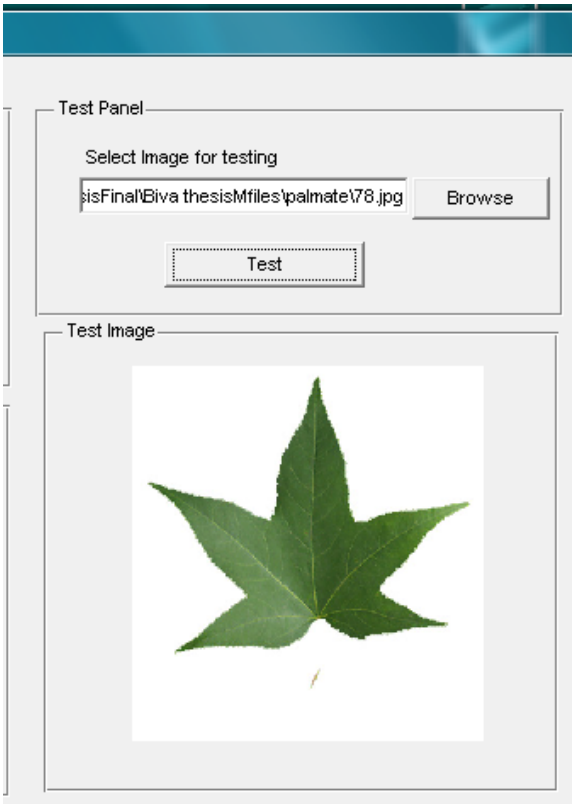

Fig. A.4: The Test panel for AppLeClass

Test Image Features

Interactions as shown in* Fig. A.5*:

- The extraction of convex hull and aspect ratio is shown in the first figure
- The extraction of eccentricity is shown in the second figure
- The extraction of skeleton in high threshold is shown in the third figure
- The extraction of skeleton in low threshold is shown in the fourth figure
- The task bar at the lower bottom shows the task status.

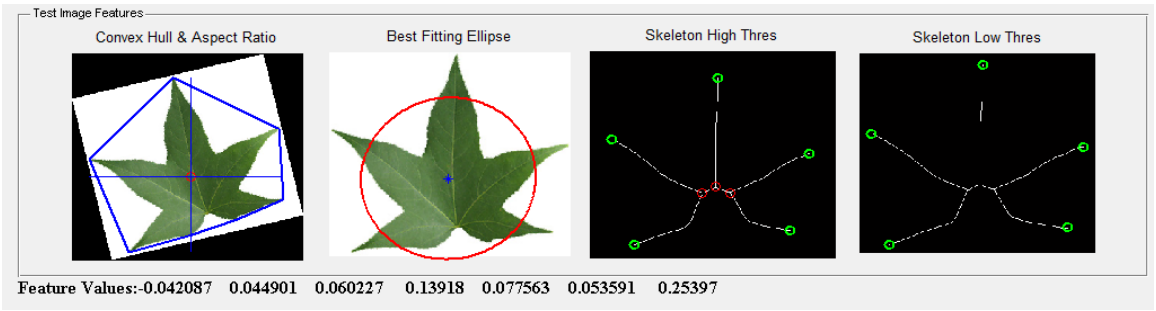

Fig. A.5: The Test Image Features panel for AppLeClass

Test results Classification:

Interactions as shown in* Fig. A.6*:

Most Probable leaves: The respective text area shows the five best matches and the image of the best match is displayed just below.

Click thumbnails to view other similar images: Below this heading other four best matches are shown in thumbnail. When the thumbnail is clicked the image is shown in the panel and a web page related to that plant also opens automatically.

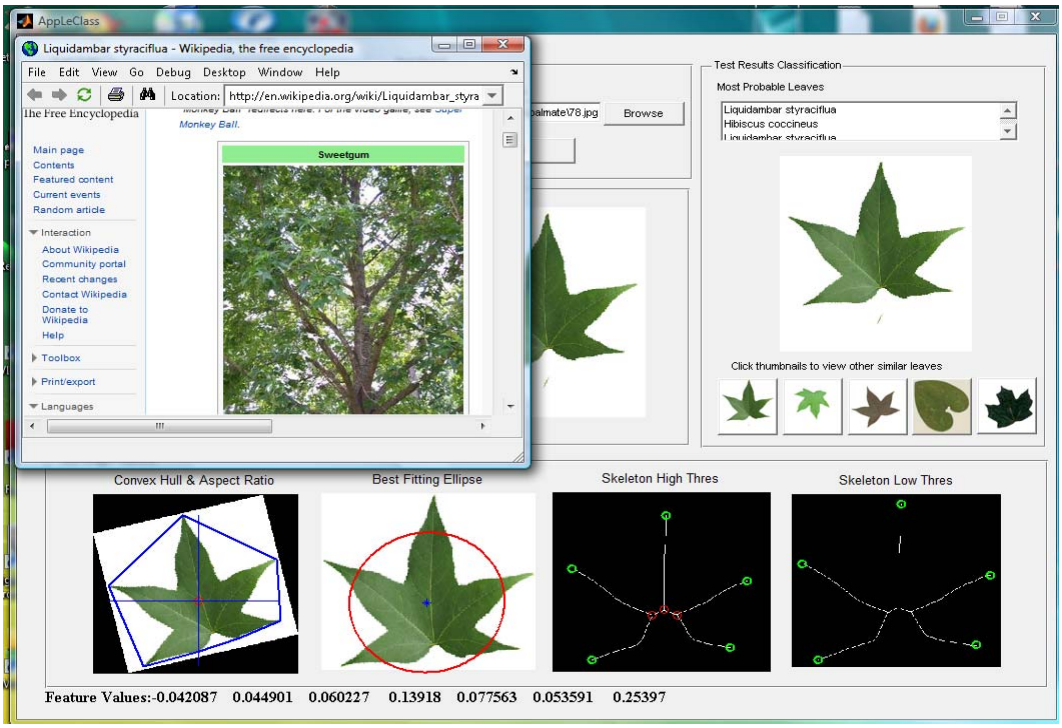

Fig. A.6: The Classification Results panel for AppLeClass

APPENDIX B

Test Data Set

Table B-1: Leaves used in the research for training classification data

Species Name	Number of leaf images	Leaf shape
Acer barbatum	2	Palmate and doubly serrated
Acer rubrum	7	Palmate and doubly serrated
Acer drummondii	1	Palmate and doubly serrated
Acer saccharum	1	Palmate and doubly serrated
Lysimachia lanceolata	4	Acicular
Palafoxia callosa	3	Acicular
Quercus phellos	3	Acicular
Anoda cristata	1	Hastate
Polygonum arifolium	3	Hastate
Hibiscus militaris	4	Hastate
Viola hastata	2	Hastate
Asarum hartwegii	1	Heart-shaped
Hexastylis arifolia	4	Heart-shaped
Hexastylis contracta	2	Heart-shaped
Hexastylis heterophylla	3	Heart-shaped
Hexastylis minor	1	Heart-shaped
Hexastylis virginica	1	Heart-shaped
Hexastylis naniflora	1	Heart-shaped
Andrachne phyllanthoides	4	Orbicular
Lonicera implexa	1	Orbicular
Orbicularia purpurea	1	Orbicular
Populus tremuloides	1	Orbicular
Saintpaulia grotei	1	Orbicular
Saintpaulia robertson	1	Orbicular
Senecio obovatus	2	Orbicular
Hibiscus coccineus	2	Palmate
Liquidambar styraciflua	6	Palmate
Malva abutilon	1	Palmate
Liriodendron tulipifera	10	Palmate

Phacelia purshii	1	Lobed
Quercus alba	1	Lobed
Quercus rubra	4	Lobed
Quercus stellata	3	Lobed
Quercus velutina	3	Lobed
Apocynum cannabinum	3	Elliptical
Apocynum medium	1	Elliptical
Vinca major	7	Elliptical
Fagus grandifolia	3	Elliptic and serrated
Castanea dentata	5	Elliptic and serrated

APPENDIX C

Sample Images

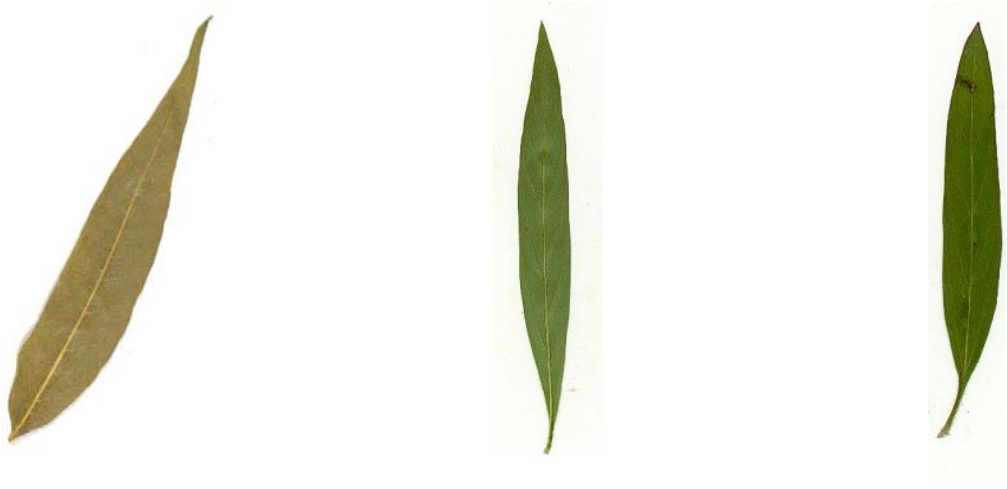

Fig. C.1: Samples of acicular leaves

Fig. C.2: Samples of hastate leaves

Fig. C.3: Samples of elliptic and singly serrated leaves

Fig. C.4: Samples of elliptic leaves

Fig. C.5: Samples of heart-shaped leaves

Fig. C.6: Samples of orbicular leaves

Fig. C.7: Samples of lobed leaves

Fig. C.8: Samples of palmate and doubly serrated leaves

Fig. C.9: Samples of palmate leaves

VITA

Ms. Biva Shrestha was born in the small city of Biratnagar, Nepal. After finishing high school in Biratnagar, she moved to the capital city of Nepal, Kathmandu to pursue a Bachelor's degree in Computer Engineering. After graduating with a Bachelor of Science Degree in Computer Engineering from Kathmandu Engineering College-Tribhuwan University in 2005, she was hired as teaching faculty in the same school for 2 years. In August 2008, she started her graduate studies at Appalachian State University, Boone, NC, USA. During the course of her graduate studies at Appalachian State University she was involved in the Summer Ventures Program in 2009 as a mentor. She will join the Oak Ridge National Lab Environmental Science Department in Knoxville, Tennessee for a Post Masters position.